Decadal–Interdecadal Climate Variability over Antarctica and Linkages to the Tropics: Analysis of Ice Core, Instrumental, and Tropical Proxy Data

YUKO M. OKUMURA

Institute for Geophysics, The University of Texas at Austin, Austin, Texas, and Climate and Global Dynamics Division, NCAR, Boulder, Colorado*

DAVID SCHNEIDER AND CLARA DESER

Climate and Global Dynamics Division, NCAR, Boulder, Colorado*

ROB WILSON

School of Geography and Geosciences, University of St Andrews, St Andrews, United Kingdom

(Manuscript received 18 January 2012, in final form 3 May 2012)

ABSTRACT

The Antarctic continent contains the majority of the global ice volume and plays an important role in a changing climate. The nature and causes of Antarctic climate variability are, however, poorly understood beyond interannual time scales due to the paucity of long, reliable meteorological observations. This study analyzes decadal–interdecadal climate variability over Antarctica using a network of annually resolved ice core records and various instrumental and tropical proxy data for the nineteenth and twentieth centuries. During the twentieth century, Antarctic ice core records indicate strong linkages to sea surface temperature (SST) variations in the tropical Pacific and Atlantic on decadal–interdecadal time scales. Antarctic surface temperature anomalies inferred from the ice cores are consistent with the associated changes in atmospheric circulation and thermal advection. A set of atmospheric general circulation model experiments supports the idea that decadal SST variations in the tropics force atmospheric teleconnections that affect Antarctic surface temperatures. When coral and other proxies for tropical climate are used to extend the analysis back to 1799, a similar Antarctic–tropical Pacific linkage is found, although the relationship is weaker during the first half of the nineteenth century. Over the past 50 years, a change in the phase of Pacific and Atlantic interdecadal variability may have contributed to the rapid warming of the Antarctic Peninsula and West Antarctica and related changes in ice sheet dynamics.

1. Introduction

The Antarctic ice sheets contain as much as 87% of the world's ice volume, an amount equivalent to 57 m of sea level rise (Lythe et al. 2001). Over the past several decades, ice shelves on the Antarctic Peninsula retreated dramatically in association with surface warming (Vaughan and Doake 1996). Following the collapse of Larsen B ice shelf in 2002, inland glaciers accelerated between twofold and eightfold due to the removal of the buttressing ice shelf (Scambos et al. 2004; Rignot et al. 2004). Changes in atmospheric circulation have likely driven increased upwelling of circumpolar deep water along the West Antarctic coast, contributing to basal melting of ice shelves and acceleration of inland glaciers (Payne et al. 2004; Thoma et al. 2008; Steig et al. 2012; Pritchard et al. 2012). Estimates based on satellite observations indicate that the West Antarctic ice sheet has been losing mass during recent decades (Zwally et al. 2005; Rignot et al. 2008; Chen et al. 2009). The associated changes in the coastal freshwater flux may also impact Antarctic Bottom Water formation and the global thermohaline circulation (e.g., Rintoul 2007;

* The National Center for Atmospheric Research is sponsored by the National Science Foundation.

Corresponding author address: Yuko M. Okumura, Institute for Geophysics, The John A. and Katherine G. Jackson School of Geosciences, The University of Texas at Austin, J. J. Pickle Research Campus, Bldg. 196, 10100 Burnet Rd., Austin, TX 78758.
E-mail: yukoo@ig.utexas.edu

DOI: 10.1175/JCLI-D-12-00050.1

Sen Gupta et al. 2009; Weaver et al. 2003). Thus, Antarctic climate change is not a regional issue but has important global implications.

The surface temperature warming in the Antarctic Peninsula region has been in part associated with an upward trend of the southern annular mode (SAM) (e.g., Thompson and Solomon 2002; Marshall 2007). The SAM represents variability of the westerly circumpolar vortex and is characterized by a seesaw pattern of pressure anomalies between the polar and midlatitude regions (Thompson and Wallace 2000). During the positive phase of the SAM, intensified westerly winds advect relatively warm oceanic air over the peninsula while surface temperature decreases in the continent interior due to a suppression of the katabatic flow over the polar cap (van den Broeke and van Lipzig 2004). Although the SAM is regarded as an internal mode of atmospheric variability (Limpasuvan and Hartmann 2000), atmospheric and climate model studies suggest that both stratospheric ozone depletion and greenhouse gas increases caused an upward trend in the SAM index over recent decades (e.g., Gillett and Thompson 2003; Shindell and Schmidt 2004; Arblaster and Meehl 2006; Miller et al. 2006; Cai and Cowan 2007; Deser and Phillips 2009; Polvani et al. 2011; Thompson et al. 2011). The forced SAM change is strongest in austral summer and autumn, when this mode is coupled to the circulation of the lower stratosphere. (Seasons refer to those in the Southern Hemisphere hereafter.)

By reconstructing spatially complete surface temperature data based on in situ and satellite observations, Steig et al. (2009) showed that the strong warming trend is not confined to the Antarctic Peninsula but extends over most of West Antarctica. The West Antarctic warming exceeds 0.1°C per decade over the past 50 years and is strongest in winter and spring. The spatial pattern and seasonality of this Antarctic warming cannot be explained by the anthropogenic change in SAM, which induces cooling over West Antarctica. An atmospheric model forced by observed history of sea surface temperature (SST) and sea ice successfully simulates the West Antarctic warming over the past 50 years while the same model coupled to an ocean model fails to reproduce the observed trend pattern (Steig et al. 2009). Schneider et al. (2012a) show that the spring warming over West Antarctica is a robust feature in many other Antarctic temperature datasets and that the associated change in atmospheric circulation can be simulated in an atmospheric model forced by observed SSTs. Ding et al. (2011) suggest that SST warming in the central tropical Pacific caused the West Antarctic warming during winter by forcing an atmospheric circulation change in the Amundsen Sea over the past 30 years.

On interannual time scales, tropical Pacific SST variations associated with the El Niño–Southern Oscillation (ENSO) are known to affect Antarctica via atmospheric teleconnections [for a review, see Turner (2004)]. A change in tropical precipitation and resultant latent heat release forces an atmospheric barotropic Rossby wave into the extratropics, where it modifies circulation patterns through interactions with transient eddies along the storm tracks (e.g., Trenberth et al. 1998). Over the South Pacific sector, a Rossby wave train often extends from the subtropics poleward and eastward to South America during ENSO evens, a configuration that is termed the Pacific–South American (PSA) pattern (e.g., Mo and Ghil 1987; van Loon and Shea 1987; Karoly 1989; Kidson 1999). The ENSO teleconnections to the Southern Hemisphere are strongest in winter and spring, preceding the peaks of ENSO events by one season, due to the seasonality of the background atmospheric circulation (Jin and Kirtman 2009). During El Niño events, a high pressure anomaly develops over the Amundsen–Bellingshausen Sea as part of the PSA pattern, inducing a zonal dipole pattern of surface temperature and precipitation anomalies over the Pacific and Atlantic sectors of Antarctica (Yuan and Martinson 2001; Kwok and Comiso 2002; Ribera and Mann 2003; Bromwich et al. 2004; Lee et al. 2010; Schneider and Steig 2002; Schneider et al. 2012b). Several studies suggest that the ENSO–Antarctic teleconnection pattern exhibits decadal variability (Bromwich et al. 2000; Fogt and Bromwich 2006). Tropical Pacific SST variations on decadal–interdecadal time scales are expected to affect the Southern Hemispheric circulation through similar mechanisms (e.g., Garreaud and Battisti 1999; Salinger et al. 2001; Mo 2000; Villalba et al. 2011), but their impact on Antarctic climate is not well documented. Decadal–interdecadal climate variations in the Atlantic basin may also influence Antarctica (Chylek et al. 2010), as suggested from studies of millennial climate variability during the last glacial–deglacial period (e.g., Timmermann et al. 2010) although detailed teleconnection mechanisms are not clear.

The pattern and amplitude of a climate trend can be significantly influenced by the presence of natural, low-frequency climate variability when the data record is not sufficiently long. Most Antarctic research stations did not start reporting surface meteorological observations until the 1957–58 International Geophysical Year. These stations are mostly located near the coast with a large void in West Antarctica, the Pacific sector of Antarctica. There is no year-round research station between Scott Base (77.9°S, 166°E) and Rothera Research Station (67.5°S, 68.1°W) and over Marie Byrd Land, where a significant warming trend has been reported. The automated weather station network and satellite observations fill

this gap in spatial data coverage but they did not begin until the early 1980s (e.g., Chapman and Walsh 2007; Comiso 2000). Because of the sparseness and short duration of the observational network, the nature and causes of Antarctic climate variability beyond interannual time scales are poorly understood.

Annually resolved ice core records spanning the last few centuries are becoming increasingly available across the Antarctic continent, offering a unique opportunity to analyze decadal–interdecadal climate variability. In particular, a recent drilling project, the International TransAntarctic Scientific Expedition (ITASE) (Steig et al. 2005), provided precisely dated records of water stable isotopes at very fine depth resolution from high accumulation rate sites over the West Antarctic ice sheet where in situ meteorological observations are few. Despite the complexities in the processes that control isotopic fractionation, most isotope modeling studies have upheld the traditional interpretation of isotope anomalies as indicators of local temperature during precipitation (Jouzel et al. 1997; Werner and Heimann 2002). Noone (2008) suggests that changes in large-scale atmospheric circulation bring about synchronous changes in local temperature and moisture transport. Although individual ice cores are subject to noise unrelated to local weather and climate, such as blowing of snow, covarying signals in multiple ice cores are associated with dominant patterns of atmospheric circulation variability (e.g., Fisher 2002; Schmidt et al. 2007; Schneider and Noone 2007).

This is one of the first comprehensive studies to analyze spatial patterns of Antarctic variability on decadal and interdecadal time scales and their linkages to global climate. We utilize a network of 17 ice core records from the Antarctic continent in conjunction with global instrumental datasets and tropical proxy records to address the following questions. What are the dominant patterns of decadal–interdecadal climate variability over Antarctica? Are they linked to climate variations in other regions of the globe? What are the potential physical mechanisms for the linkages? Is the Antarctic temperature trend over recent decades influenced by low-frequency variability?

We first conduct simple correlation analysis between ice core records and global instrumental data during the twentieth century, without any a priori assumptions of the patterns of variability. Next, more objective statistical analyses are conducted to extract robust patterns of covariability between Antarctic and tropical climate. A set of atmospheric model simulations is also analyzed to investigate mechanisms of the teleconnections. We then extend the analysis back to the nineteenth century by using a network of coral and other proxy records from the tropics to test if the knowledge obtained from the analyses of ice core and instrumental data holds true for the past two centuries.

The paper is organized as follows. Section 2 describes the ice core and various observational and tropical proxy data used in this study. Section 3 analyzes the relationships between Antarctic and tropical climate variability during the twentieth century. The teleconnection mechanisms are investigated in section 4. Section 5 extends the analysis presented in section 3 to the nineteenth century by using tropical proxy records. Summary and discussion are provided in section 6.

2. Data, model, and methods

a. Ice cores

A set of 17 Antarctic ice core records (including one snow pit record from Vostok) is used to assess Antarctic climate variability. We use annual-mean records of water isotopes (δ^{18}O or δD) that begin in 1900 or earlier and end in 1981 or later. In this study, the annual mean is defined for the calendar year (January–December). There are six records that extend back to at least 1799. Table 1 summarizes the names, locations, available periods, and types of ice core records. Figure 1 indicates the locations of ice cores available for 1900–81 by light blue circles and for 1799–1981 by dark blue circles. These ice cores are distributed across the Antarctic continent with about half over the West Antarctic ice sheet. All but two records were compiled by Schneider and Noone (2007) and described in references therein. The first additional record is from Gomez (73.6°S, 70.4°W), provided by E. R. Thomas and described in Thomas et al. (2009); the second additional record is from Dolleman Island (70.3°S, 60.5°W), provided by R. Mulvaney and described in Peel et al. (1988). Figure 2 overlays the locations of ice cores on annual surface mass balance (precipitation minus sublimation and snowmelt, van de Berg et al. 2006). The surface mass balance varies considerably from location to location, which may affect the time scales resolved by individual ice core records. In general, a snow accumulation rate over 100 mm yr^{-1} is required to recover an annual time series. Most of the ice cores, except a few from East Antarctica, satisfy this criterion.

To compare the time scales of variability in individual ice core records, temporal autocorrelations at 1-yr lag are shown for 1900–99 in Fig. 3. These values are also compared with the autocorrelation of annual SST anomalies in the Niño-3.4 region (5°S–5°N, 120°–170°W), an index for ENSO, one of the dominant forcings of interannual variability over Antarctica. The ice cores in

TABLE 1. List of 17 Antarctic ice core records used in this study. The labels correspond to those in Fig. 1. Bolded names indicate records available from 1799 or earlier.

Label	Name	Lat	Lon	Period	Type
A	Vostok snow pit	78.00°S	106.00°E	1900–99	δD
B	Law Dome 2000	66.78°S	112.82°E	1900–99	δ^{18}O stack
C	**Talos Dome**	72.80°S	159.75°E	1750–1999	δD
D	Siple Dome A	81.65°S	148.81°W	1900–93	δD
E	**ITASE 00–5**	77.68°S	123.99°W	1750–1999	δD
F	**ITASE 00–1**	79.38°S	111.23°W	1750–1999	δD
G	**ITASE 02–4**	86.50°S	107.99°W	1753–1998	δD
H	ITASE 01–2	77.84°S	102.91°W	1900–99	δ^{18}O
I	ITASE 01–3	78.12°S	95.65°W	1900–99	δD
J	**ITASE 01–5**	77.06°S	89.14°W	1799–2001	δ^{18}O
K	**Siple Station**	75.92°S	84.15°W	1750–1983	δ^{18}O
L	Gomez	73.59°S	70.36°W	1857–2005	δ^{18}O
M	Dyer Plateau	70.66°S	64.50°W	1900–89	δ^{18}O
N	Dolleman Island	70.30°S	60.50°W	1900–81	δ^{18}O
O	James Ross Island	64.20°S	57.67°W	1900–99	δ^{18}O
P	Berkner Island	79.61°S	45.72°W	1900–92	δ^{18}O
Q	Dronning Maud Land	75.00°S	0.00°W	1900–97	δ^{18}O stack

West Antarctica and the Antarctic Peninsula show autocorrelation values comparable to that of the Niño-3.4 index (0.15), consistent with the strong ENSO signals evident in these cores (Schneider et al. 2012b). Autocorrelations exceed 0.4 in low snow deposition sites over East Antarctica, indicating that these ice core records cannot resolve interannual variability and/or that the physical processes affecting these cores have longer time scales. The autocorrelation is as high as 0.76 in Vostok snow pit where annual mass balance is below 100 mm yr^{-1}. Indeed, the annual time series of the Vostok record is much smoother than those of the other cores and exhibits distinct decadal–interdecadal variations (not shown).

b. *Global instrumental datasets*

A suite of global, monthly instrumental datasets is used to analyze patterns of large-scale climate variability associated with isotope anomalies in the Antarctic ice core records. For SST we use the Hadley Centre Sea Ice and SST (HadISST) (Rayner et al. 2003) available on a 1° grid for 1870–2010. It is based on historical in situ ship and buoy observations with satellite data blended in after 1982. Missing grid boxes are filled by optimal interpolation based on empirical orthogonal function (EOF) analysis. For precipitation we use the dataset from the Climate Research Unit of the University of

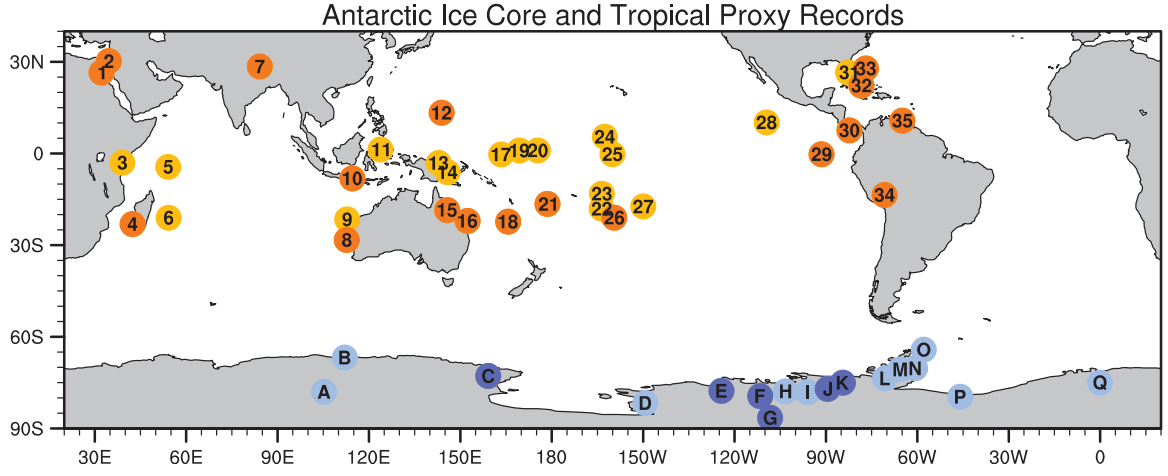

FIG. 1. Locations of Antarctic ice core (light and dark blue circles) and tropical proxy (yellow and orange circles) records used in this study. The labels correspond to those in Tables 1 and 2. The light blue and yellow circles indicate the records available for 1900–81, and the dark blue and orange circles indicate the records available for 1799–1981. For visual clarity, the locations of some tropical proxy records are slightly offset.

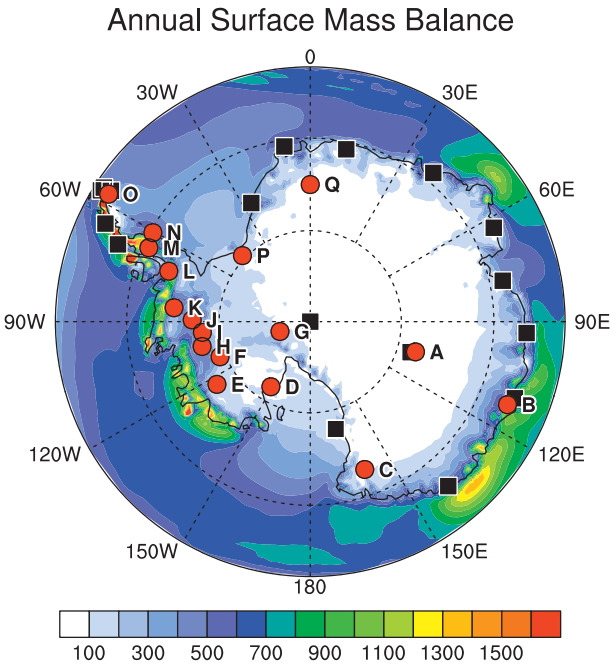

FIG. 2. Annual-mean surface mass balance in Antarctica (mm water equivalent per year; shading; van de Berg et al. 2006). The red circles indicate the locations of ice core records. The labels correspond to those in Table 1. For reference, the black squares indicate the locations of year-round research stations where in situ meteorological observations are available since 1957.

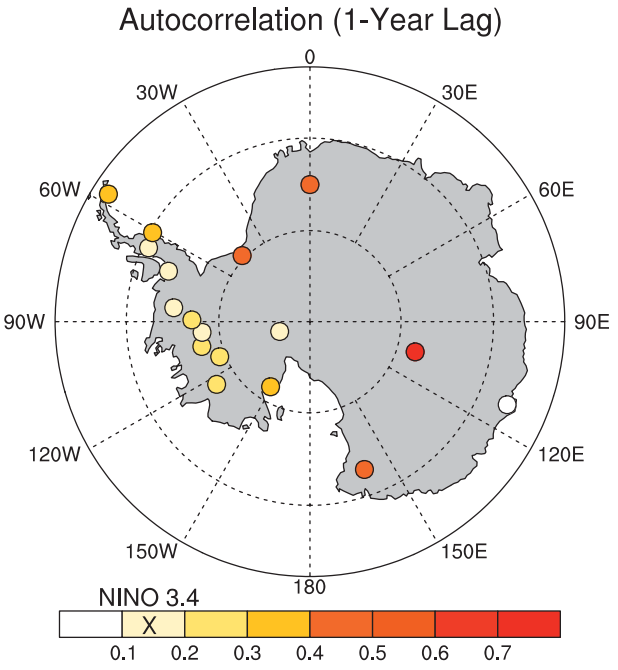

FIG. 3. Autocorrelations of unsmoothed ice core records at 1-yr lag for 1900–99. The cross on the label bar indicates the autocorrelation of annual Niño-3.4 SST index at 1-yr lag for the same period (0.15).

East Anglia (Hulme et al. 1998) available on a 2.5° latitude × 3.75° longitude grid for 1900–98. It is based on land station records and no interpolation has been conducted to fill in missing grid values. Although the precipitation data are not available over the ocean, coastal and island stations provide some information on changes in large-scale marine precipitation patterns. For sea level pressure (SLP) we use the Hadley Center SLP version 2 (HadSLP2) (Allan and Ansell 2006) available on a 5° grid for 1850–2004. The HadSLP2 is a globally complete reconstruction based on terrestrial station records and marine observations. These independent datasets show physically consistent variability over the tropical Pacific on interannual to interdecadal time scales (Deser et al. 2004, 2010b).

c. *Tropical proxies*

As will be shown in the next section, Antarctic ice core records exhibit strong linkages to tropical climate variations during the twentieth century. To extend the analysis of such linkages back to the nineteenth century, we utilize various proxy records of tropical climate that are available at annual temporal resolution and span different periods during the nineteenth and twentieth centuries. We use 35 tropical proxy records available for 1900–81, 18 of which extend back to at least 1799. The majority of these proxies are δ^{18}O isotopic records from corals and the others include coral luminescence, coral growth rate, tree ring, ocean sediment, and tropical ice core. These records represent various elements of tropical climate such as SST, salinity, river discharge, air temperature, precipitation, and wind-induced ocean upwelling. Table 2 summarizes the information on tropical proxy records. Figure 1 indicates the locations of tropical proxies available for 1900–81 by yellow circles and for 1799–1981 by orange circles. All but two records were compiled by Wilson et al. (2010) and are described in references therein. We added two records from the tropical Atlantic described in Black et al. (1999) and Saenger et al. (2009). For display purposes, we reversed the sign of coral isotope and ocean sediment records that are negatively correlated with local SST anomalies.

d. *Atmospheric model*

To test the hypothesized mechanism of Antarctic–tropical linkages, we analyze ensemble atmospheric model simulations forced with observed monthly SSTs. The model used for these simulations is the Community Atmosphere Model version 3 (CAM3) (Collins et al. 2006) at a horizontal resolution of T85 (~1.4° latitude × 1.4° longitude) with 26 vertical levels. The observed monthly SSTs are prescribed over both the global

TABLE 2. List of the 35 tropical proxy records used in this study. The labels correspond to those in Fig. 1. Bolded names indicate records available from 1799 or earlier.

Label	Name	Lat	Lon	Period	Type
1	**Ras Umm Sidd**	27.50°N	34.18°E	1751–1995	Coral $\delta^{18}O$
2	**Aqaba**	29.26°N	34.58°E	1788–1992	Coral $\delta^{18}O$
3	Malindi	3.00°S	40.00°E	1801–1992	Coral $\delta^{18}O$
4	**Madagascar (Ifaty)**	23.09°S	43.34°E	1660–1995	Coral $\delta^{18}O$
5	Mahe, Seychelles	4.37°S	55.00°E	1846–1995	Coral $\delta^{18}O$
6	St. Gilles, La Réunion	21.02°S	55.15°E	1832–1995	Coral $\delta^{18}O$
7	**Nepal**	28.50°N	85.00°E	1546–1991	Tree ring
8	**Houtman Abrolhos Island**	28.28°S	113.46°E	1794–1994	Coral $\delta^{18}O$
9	Ningaloo Reef	21.54°S	113.58°E	1879–1994	Coral $\delta^{18}O$
10	**Lombok Straight**	8.15°S	115.30°E	1782–1989	Coral $\delta^{18}O$
11	Bunaken Island	1.30°N	124.50°E	1860–1989	Coral $\delta^{18}O$
12	**Guam**	13.36°N	144.50°E	1790–2000	Coral $\delta^{18}O$
13	Laing Island	4.09°S	144.53°E	1885–1992	Coral $\delta^{18}O$
14	Madang Lagoon	5.13°S	145.49°E	1881–1992	Coral $\delta^{18}O$
15	**Havannah Island**	18.51°S	146.33°E	1644–1986	Coral luminescence
16	**Abraham Reef**	22.06°S	153.00°E	1638–1983	Coral $\delta^{18}O$
17	Nauru Island	0.30°S	166.00°E	1897–1994	Coral $\delta^{18}O$
18	**New Caledonia**	22.29°S	166.27°E	1658–1992	Coral $\delta^{18}O$
19	Tarawa	1.00°N	172.00°E	1894–1988	Coral $\delta^{18}O$
20	Maiana	1.00°N	173.00°E	1840–1994	Coral $\delta^{18}O$
21	**Fiji**	16.49°S	179.14°E	1776–2001	Coral $\delta^{18}O$
22	Palmerston	18.03°S	163.12°W	1834–1998	Coral $\delta^{18}O$
23	Suwarrow Atoll	13.15°S	163.06°W	1881–1998	Coral $\delta^{18}O$
24	Palmyra Island	5.52°N	162.08°W	1886–1996	Coral $\delta^{18}O$
25	Jarvis	0.22°S	159.59°W	1850–1998	Coral $\delta^{18}O$
26	**Rarotonga**	21.00°S	159.00°W	1726–1996	Coral $\delta^{18}O$
27	Moorea	17.30°S	149.50°W	1852–1990	Coral $\delta^{18}O$
28	Clipperton Atoll	10.18°N	109.13°W	1894–1993	Coral $\delta^{18}O$
29	**Urvina Bay**	0.24°S	91.14°W	1607–1981	Coral $\delta^{18}O$
30	**Secas Island**	7.59°N	82.03°W	1708–1983	Coral $\delta^{18}O$
31	Florida Bay	24.56°N	80.45°W	1824–1985	Coral $\delta^{18}O$
32	**Alina's Reef (Biscayne National Park)**	24.25°N	80.10°W	1751–1986	Coral $\delta^{18}O$
33	**Bahamas**	25.84°N	78.62°W	1552–1991	Coral growth rate
34	**Quelccaya**	13.56°S	70.50°W	1540–2002	Ice core
35	**Cariaco Basin**	10.76°N	64.69°W	1116–1990	Ocean sediment

domain and the tropics (20°S–20°N) only. These simulations are referred to as the Global Ocean and Global Atmosphere (GOGA) and Tropical Ocean and Global Atmosphere (TOGA) runs, respectively, following convention (e.g., Lau and Nath 1994). In the TOGA run, climatological monthly SSTs are prescribed poleward of 30° latitude while monthly SSTs are linearly blended with climatological monthly SSTs over the latitude band 20°–30° in both hemispheres. The GOGA and TOGA ensembles each consist of five integrations and are available for 1950–2008 and 1871–2000, respectively. We analyze the ensemble mean fields of surface air temperature, precipitation, and SLP. See Deser and Phillips (2009) for further information on these simulations.

e. Methods

For a given analysis period, annual or monthly climatologies are removed from all data. The monthly anomalies of instrumental data and CAM3 output are then converted into annual means by taking an average from January through December for each year. At least four months of data are required to calculate annual-mean anomalies of the Hulme et al. (1998) precipitation that contains missing values. To reduce interannual variability associated with ENSO, we apply a three-point binominal (1–2–1) temporal filter to all annual data. Secular trends are then removed based on least squares quadratic regression analysis. Using linear instead of quadratic regression to estimate the trend does not significantly alter the main results for the twentieth century alone but can be problematic for the extended period including the nineteenth century, during which some tropical proxy records exhibit trends departing from linearity. The HadISST and HadSLP2 data are also spatially smoothed with a local nine-point filter to reduce small-scale noise. Finally, the ice core and tropical

proxy records are standardized to have a mean of zero and standard deviation of one. The temporal filtering and standardization serve to reduce the inhomogeneity in types and effective temporal resolutions of these proxy records. Although climate reconstruction studies often prescreen proxy records for correlation with local climate parameters (e.g., Wilson et al. 2010), we use all the available proxy records and attempt to extract the patterns of covarying signals.

To quantify the relationships between Antarctic ice core records and global climatic fields, we conduct linear temporal correlation analysis. The statistical significance of the resulting correlation coefficients is assessed by a one-tailed Student's t test. For simplicity, the effective sample size (N_{eff}) is estimated by dividing the number of years by the mean characteristic time scale (τ) of annual anomalies smoothed with a three-point binomial filter. We define τ as a minimum lag for which the autocorrelation falls below 0.2. On average, τ is largest for SST (5.4 yr) compared to 2.9 yr for the ice cores and 3.4 yr for precipitation. A correlation coefficient that exceeds 0.37 and 0.27 in absolute value is significantly different from 0 at the 95% confidence level for record lengths of 100 years ($N_{\text{eff}} = 19$) and 200 years ($N_{\text{eff}} = 37$), respectively. Besides the simple significance test, we rely on physical consistency among variables from independent sources and robustness of the results in various analyses. To more objectively analyze the dominant patterns of covariability between ice cores and tropical SSTs or proxies, we also conduct singular value decomposition (SVD) analysis (Bretherton et al. 1992; Wallace et al. 1992). The SVD analysis is a multivariate statistical technique widely used in climate research to isolate linearly related spatial patterns in two fields by decomposing the cross-covariance matrix into singular vectors.

3. Antarctic–tropical linkages during the twentieth century

a. Correlation analysis

What are the patterns of SST anomalies associated with decadal–interdecadal climate variations over Antarctica? Figure 4 shows one-point correlation maps between a given ice core record and the remaining 16 ice cores and global SSTs during 1900–99. All of the ice core records exhibit distinct large-scale SST correlation patterns, especially over the tropical oceans. Talos Dome and several cores in central West Antarctica (ITASE 00–5, 00–1, 01–2, and 01–3) show significant positive SST correlations in the tropical Pacific and Indian Ocean and negative correlations in the central North Pacific. The area of positive SST correlations extends into the subtropics over the eastern Pacific, along the west coast of North America, and as far as the Gulf of Alaska. This horseshoe pattern of SST correlations in the North Pacific is reminiscent of the anomaly pattern associated with the Pacific decadal oscillation (PDO) or interdecadal Pacific oscillation (e.g., Mantua et al. 1997; Zhang et al. 1997; Garreaud and Battisti 1999; Power et al. 1999; Salinger et al. 2001; Deser et al. 2004, 2010a). These ice core records that exhibit similar SST correlation patterns are, in general, positively correlated with each other. ITASE 02–4 also shows a SST correlation pattern suggestive of the PDO with the sign reversed.

Many ice cores in the peninsula and eastern West Antarctica exhibit organized patterns of SST correlation in the Atlantic basin (Fig. 4). In particular, ITASE 01–5, Siple Station, Gomez, Dolleman Island, and James Ross Island show a meridional dipole pattern of SST correlation between the North and South Atlantic, indicating that positive isotope anomalies in these cores tend to occur with positive SST anomalies in the tropical South Atlantic and negative SST anomalies over most of the North Atlantic and vice versa. The ITASE 01–5 and Dolleman Island show significant negative SST correlations to the south of Iceland. This basin-scale pattern of SST correlation bears some resemblance to the anomaly pattern associated with the Atlantic multidecadal oscillation (AMO) (e.g., Delworth and Mann 2000, Enfield et al. 2001; Guan and Nigam 2009; Deser et al. 2010a) although all of these ice core records exhibit stronger correlation with SSTs in the tropical South Atlantic than in the North Atlantic. The dipole pattern of SST correlation in the tropics is also reminiscent of the meridional mode of tropical Atlantic variability on interannual–decadal time scales (e.g., Nobre and Shukla 1996; Chang et al. 1997; Okumura et al. 2001; Xie and Carton 2004). Among the remaining cores, Vostok snow pit shows significant negative correlations with North Atlantic SSTs and positive correlations with tropical Indian Ocean SSTs. The SST correlation map for Dronning Maud Land projects onto the positive phases of both the PDO and AMO although the correlations are weak overall. Dyer Plateau and Berkner Island do not exhibit a coherent pattern of SST correlation that resembles a known pattern of climate variability. Some ice core records (e.g., Gomez and Dolleman Island) are strongly correlated with SSTs in the high-latitude Southern Ocean. However, we note that in situ SSTs are very poorly sampled in this region throughout the twentieth century (e.g., Deser et al. 2010a).

The simple correlation analysis suggests that decadal–interdecadal variations in Antarctic ice core records are

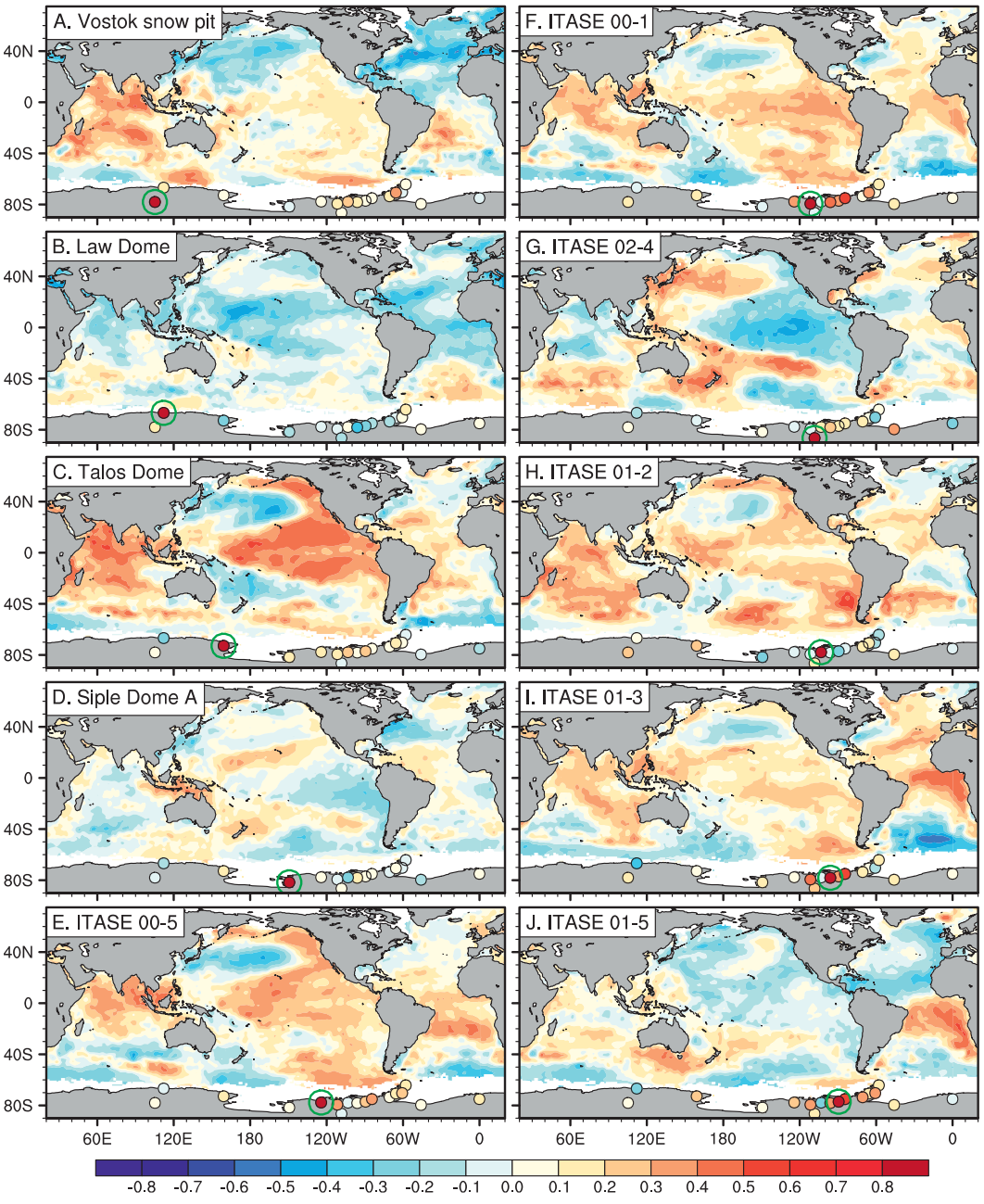

FIG. 4. One-point correlation maps between a given ice core record (identified by name in the upper left corner and marked by a green circle) and the remaining 16 ice cores (circles) and global SSTs (shading) during 1900–99. The color bar applies to both SST and ice core correlation coefficients. The panels are arranged by increasing longitude.

linked with basin-scale SST variations, particularly in the tropical Pacific and Atlantic. We ask, in turn, what are the dominant patterns of tropical SST variability and how are they related to the ice core records? Figure 5a shows the leading EOF and associated principal component (PC) time series of tropical Indo-Pacific SSTs (30°S–30°N, 30°E–80°W) for 1900–81. This mode represents the tropical extension of the PDO. The PC time series indicates decadal–interdecadal variations with predominantly positive and negative phases alternating every two to three decades. Figure 5b shows the leading EOF and associated PC time series of tropical Atlantic SSTs (30°S–30°N, 80°W–30°E) for 1900–81. To isolate tropical Atlantic variability that is independent

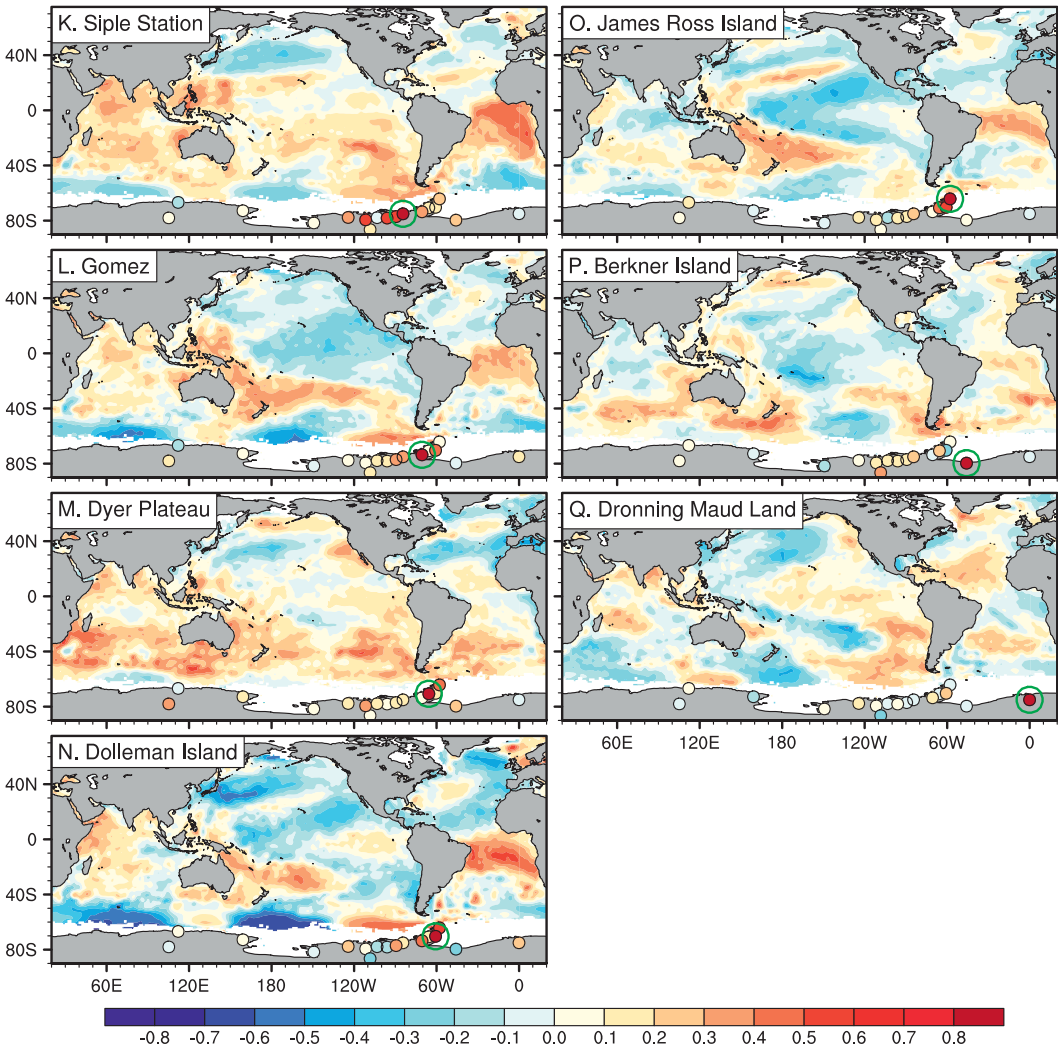

FIG. 4. (*Continued*)

of the tropical Pacific, linear regressions onto the leading PC of tropical Indo-Pacific SSTs are removed from Atlantic SSTs prior to the EOF analysis. This mode exhibits a dipole pattern between the North and South Atlantic, similar to the meridional mode of tropical Atlantic variability. The PC time series is dominated by decadal variability during the first 40 yr, followed by a prolonged positive phase and a rapid transition to a negative phase in the early 1970s.

Based on the leading EOF patterns of tropical Indo-Pacific and Atlantic SSTs, we define simple indices to represent Pacific decadal–interdecadal variability as SST anomalies averaged in the southeast tropical Pacific (5°–20°S, 140°–90°W; rectangle in Fig. 5a) and Atlantic decadal–interdecadal variability as differences in zonal mean SST anomalies in the northern and southern tropical Atlantic (5°–25°N, 65°–15°W minus 0°–20°S, 40°W–10°E; rectangles in Fig. 5b; note that the node of the meridional SST dipole is located north of the equator). These SST indices are highly correlated with the leading PCs at coefficients of 0.90 for Pacific variability and 0.86 for Atlantic variability. The advantage of using indices instead of PCs is that they may be easily defined for different analysis periods and can be extended to the present.

Figure 6 shows correlation maps of global SSTs, land station precipitation, and ice core records with the Pacific and Atlantic SST indices for 1900–99. The SST correlation map based on the Pacific SST index exhibits a familiar pattern of the PDO, which is similar to the one-point correlation maps based on Talos Dome and several ice core records in central West Antarctica (Fig. 4). Across the margin of positive and negative SST correlations in the southwestern tropical Pacific, island

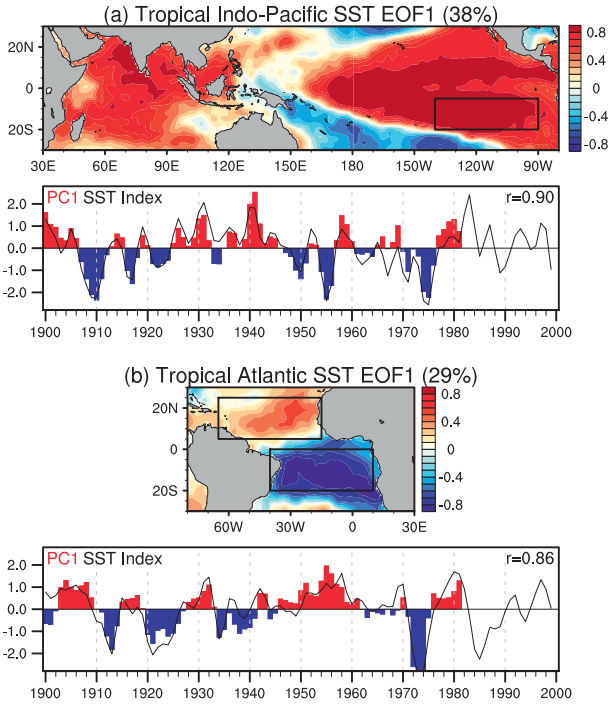

FIG. 5. (a) Leading EOF and associated time series of tropical Indo-Pacific SSTs (30°S–30°N, 30°E–80°W) for 1900–81. This mode explains 38% of the total variance. The EOF is computed from a correlation matrix. Standardized time series of the PC and Pacific SST index are shown by the color bars and black curve, respectively. The Pacific SST index is defined in the region indicated by the rectangle (5°–20°S, 140°–90°W) and shown for 1900–99. These time series are correlated at a coefficient of 0.90. (b) As in (a) but for the leading EOF and associated time series of tropical Atlantic SST (30°S–30°N, 80°W–30°E). This mode explains 29% of the total variance. Prior to the EOF analysis, linear regressions onto the leading PC of tropical Indo-Pacific SSTs are removed from Atlantic SSTs. The PC and Atlantic SST index (5°–25°N, 65°–15°W minus 0°–20°S, 40°W–10°E) are correlated at a coefficient of 0.86.

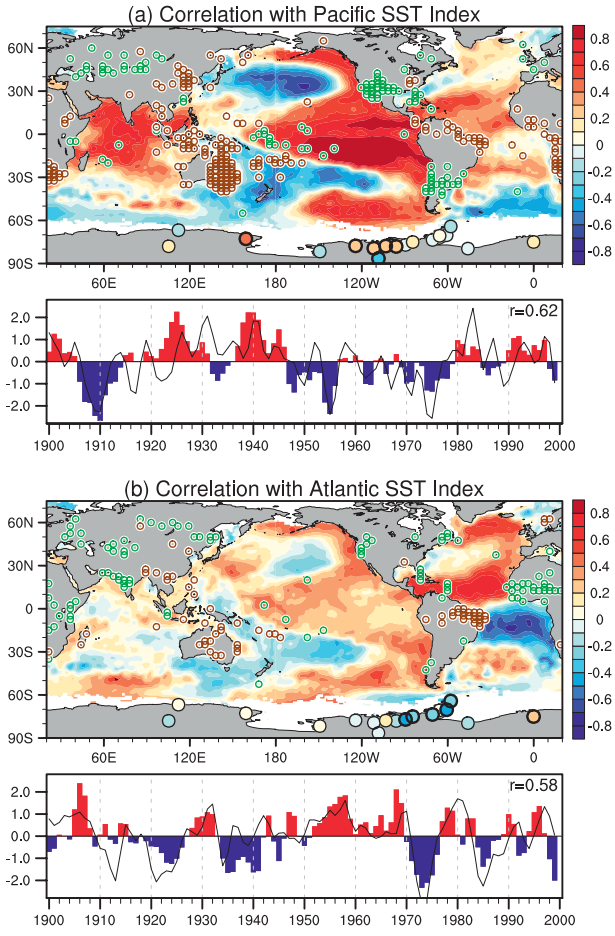

FIG. 6. (a) Pattern and time series associated with Pacific interdecadal variability. Map shows correlations of SSTs (shading), land station precipitation (brown open circles <-0.3; green open circles >0.3), and ice core records (filled circles) upon the Pacific SST index. Standardized time series of the Pacific SST and ice core indices are shown by the black curve and color bars, respectively. The ice core index is defined as a weighted average of those ice core records that exhibit correlations with the Pacific SST index greater than 0.2 in absolute value (indicated by thick black circles) using the correlation coefficients as weights. These time series are correlated at a coefficient of 0.62. (b) As in (a) but for Atlantic interdecadal variability. The Atlantic SST and ice core indices are correlated at a coefficient of 0.58.

station precipitation shows a sharp change in the sign of correlations, indicative of a meridional shift of the South Pacific convergence zone (SPCZ). Consistent with the one-point correlation analysis, the Pacific SST index is positively correlated with Talos Dome and several ice core records in central West Antarctica and negatively with the ITASE 02–4 record. The SST correlation map based on the Atlantic SST index exhibits a dipole pattern between the North and South Atlantic, similar to the one-point correlation maps based on the ice core records from the Antarctic Peninsula and eastern West Antarctica (Fig. 4). The land station precipitation shows positive correlations in the Sahel region and negative correlations in northeast Brazil, indicative of a meridional shift of the Atlantic intertropical convergence zone (ITCZ) toward the warmer hemisphere. In agreement with the one-point correlation analysis, the Atlantic SST index is negatively correlated with the ice core records in the peninsula and eastern West Antarctica. For both Pacific and Atlantic patterns, the sign of ice core correlations along the coast of Antarctica is in general consistent with the sign of SST correlations to the north although SST observations are sparse in this region before the satellite era.

We construct proxy indices of Pacific and Atlantic interdecadal variability from ice core records by computing a weighted average of those cores that exhibit correlations with the SST indices greater than 0.2 in

absolute value, using the correlation coefficients as weights. The resulting ice-core-based indices of Pacific and Atlantic interdecadal variability are significantly correlated with the SST indices at 0.62 and 0.58, respectively. For Pacific variability the prolonged negative phase from the late 1940s and rapid shift to a positive phase in the late 1970s seen in the SST index are well captured in the ice core index, although the phase shift in the mid-1920s is not very clear. For Atlantic variability the persistent positive phase from the 1940s and very rapid shift to a negative phase in the early 1970s in the SST index are also evident in the ice core index.

b. SVD analysis of ice core and tropical SST

To more objectively analyze the linkages between Antarctic and tropical climate variability, we conduct SVD analysis between the set of 17 ice core records and SSTs over the tropics (30°S–30°N) for 1900–81. Prior to conducting the SVD analysis, the SST data are aggregated onto a coarse 4° latitude × 10° longitude grid and the time series at each grid point is normalized. We obtain similar results by using fewer (9–16) ice core records to extend the analysis period up to 1983–99 (not shown). Figure 7 shows the time series of expansion coefficients and the correlation maps based on these expansion coefficients for the first and second SVD modes. These two leading modes explain 50% and 25% of the total squared covariance, well separated from the higher modes that explain less than 8%. The expansion coefficients of ice core and tropical SST are highly correlated to each other for both modes (r = 0.73 for the first mode and r = 0.75 for the second mode), indicating strong linkages between these two different fields.

To examine the global patterns associated with the two leading SVD modes, the ice core expansion coefficients are correlated with full-resolution global SSTs and land station precipitation and the expansion coefficients of tropical SST are correlated with ice core records in Fig. 7 (i.e., the heterogeneous correlation maps). The correlation map for the first mode bears a striking resemblance to the correlation map based on the Pacific SST index (cf. Figs. 6a and 7a). Indeed, the expansion coefficients of ice core and tropical SST for this mode are significantly correlated with the Pacific SST index at 0.57 and 0.90, respectively. Positive isotope anomalies at Talos Dome and in central West Antarctica are associated with positive SST anomalies in the tropical oceans. It is interesting to note that the ice core expansion coefficient shows a larger positive correlation with SSTs in the northwestern Indian Ocean than in the tropical Pacific. The correlation map for the second

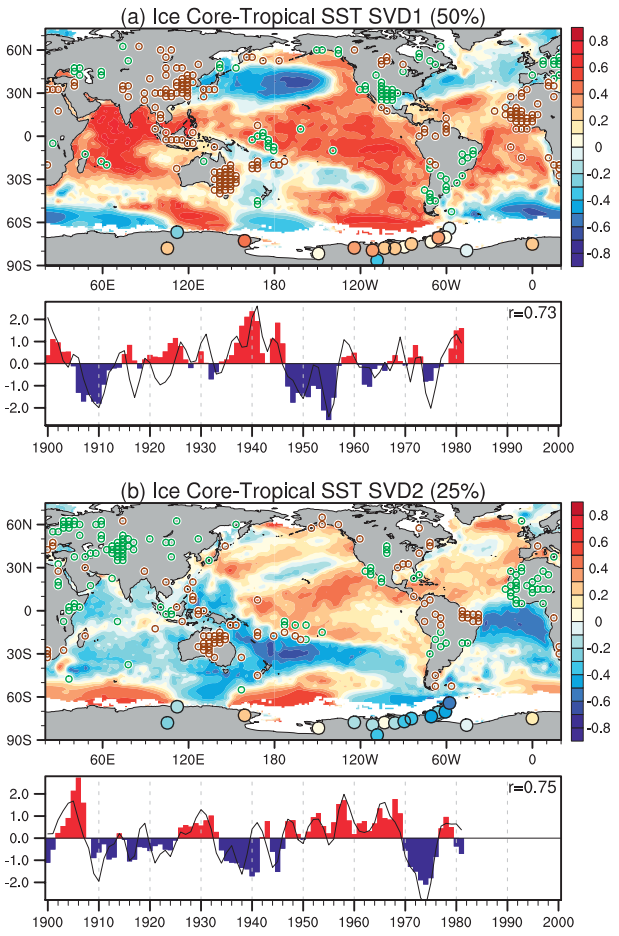

FIG. 7. (a) Pattern and time series associated with the first SVD mode of ice core and tropical SST (30°S–30°N) for 1900–81. This mode explains 50% of the total squared covariance. Map shows correlations of SSTs (shading) and land station precipitation (brown open circles <-0.3; green open circles >0.3) upon the ice core expansion coefficient and correlations of ice core records (filled circles) upon the tropical SST expansion coefficient. Although the SVD calculation is based on SSTs only in the tropics, the correlation pattern is displayed globally. Standardized time series of the ice core and tropical SST expansion coefficients are shown by the color bars and black curve, respectively. These time series are correlated at a coefficient of 0.73. (b) As in (a) but for the second SVD mode, which explains 25% of the total squared covariance. Time series of the expansion coefficients are correlated at a coefficient of 0.75.

SVD mode is very similar to the correlation map based on the Atlantic SST index (cf. Figs. 6b and 7b). The expansion coefficients of ice core and tropical SST for this mode are correlated with the Atlantic SST index at 0.55 and 0.65, respectively. Negative isotope anomalies in the peninsula and eastern West Antarctica are again associated with positive SST anomalies in the North Atlantic and negative SST anomalies in the South Atlantic. Compared to Fig. 6b, positive SST correlations in

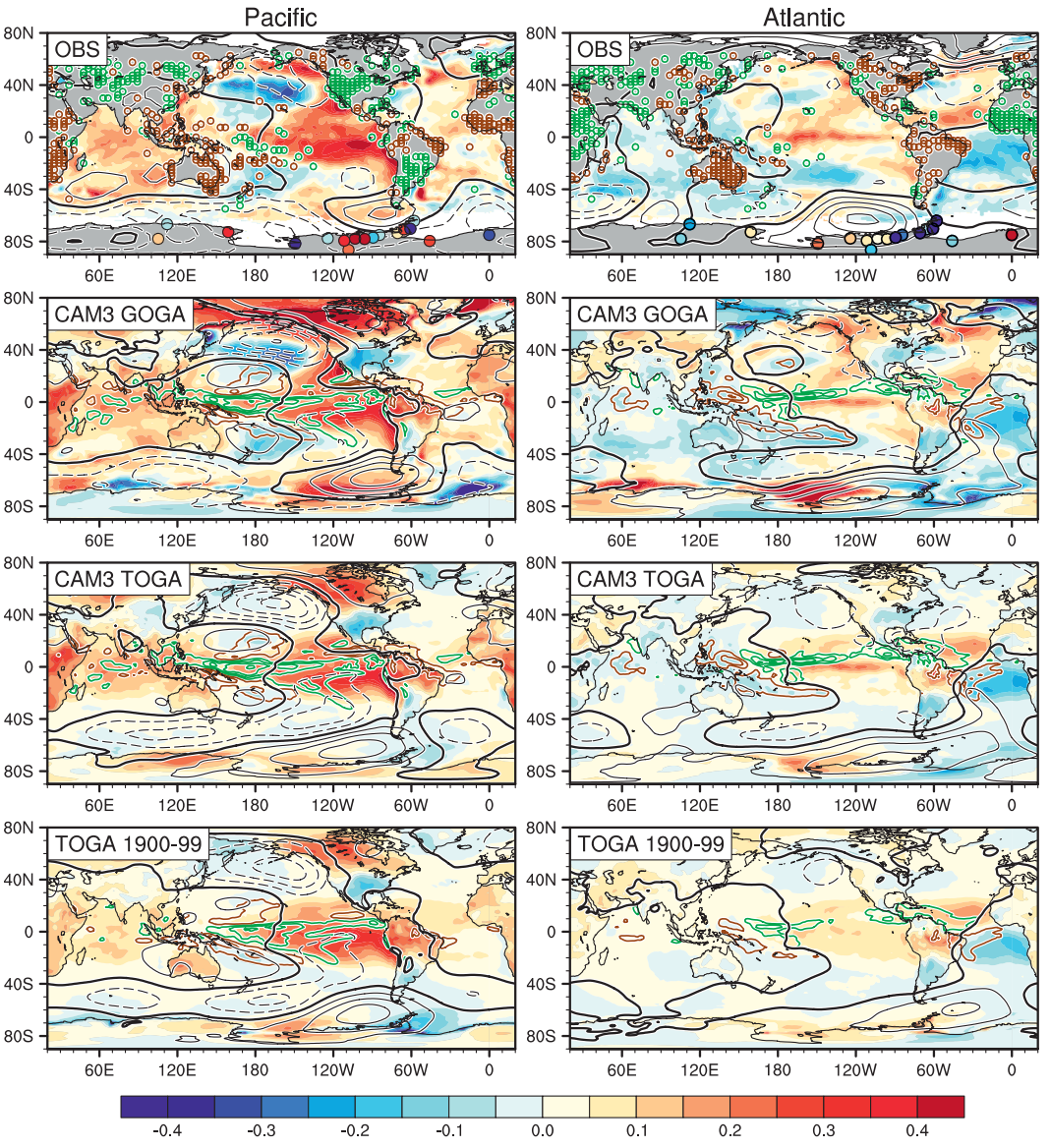

FIG. 8. Regression and correlation maps of observed and simulated anomalies upon the (left) Pacific and (right) Atlantic SST indices. (top) Regressions of observed SLP (black contours at intervals of 0.2 hPa; zero contours thickened) and SST (°C, shading) and correlations of land station precipitation (brown open circles <-0.3, green open circles >0.3) and ice core (filled circles) for 1957–99. (top middle) Regressions of SLP (black contours at intervals of 0.2 hPa; zero contours thickened), surface air temperature (°C, shading), and precipitation (negative/positive contours in brown/green at intervals of 0.3 mm day^{-1} starting from ± 0.2) simulated in the CAM3 GOGA run for 1957–99. (bottom middle) As in (top middle) but for the CAM3 TOGA run. (bottom) As in (bottom middle) but for 1900–99. In the top three rows the data are not detrended.

the northern tropical Pacific and negative SST correlations in the South Pacific and Indian Ocean are more pronounced in Fig. 7b while positive correlations in the northern tropical Atlantic weaken. The SVD analysis thus confirms the results of simple correlation analyses that decadal–interdecadal climate variability over Antarctica is strongly tied to SST variations in the tropical Pacific and Atlantic.

4. Atmospheric teleconnections

What causes the linkages between Antarctic and tropical climate variability on decadal–interdecadal time scales? Does the atmospheric Rossby wave forced by tropical precipitation changes induce surface air temperature anomalies over Antarctica, in analogy with interannual ENSO events? Are the surface air temperature

anomalies induced by the atmospheric Rossby wave consistent with isotope anomalies in Antarctic ice cores? To address these questions, SLP data are regressed onto the Pacific and Atlantic SST indices along with SSTs, land station precipitation, and ice core records in the top panels of Fig. 8. We limit the regression analysis to the period after 1957 because there are insufficient SLP observations in the high-latitude Southern Hemisphere to define large-scale patterns of variability prior to this year. We do not detrend the data before the analysis because both Pacific and Atlantic SST indices show shifts in the phase of interdecadal variability in the 1970s (Fig. 6), which would be largely effaced by detrending the data.

The regression map based on the Pacific SST index indicates that SLP increases over Indonesia and Australia and decreases over the central–eastern tropical Pacific in association with an equatorward displacement of the SPCZ during the positive phase of Pacific variability (Fig. 8, top left). This high pressure anomaly over Australia is connected with a low pressure anomaly to the south and a high pressure anomaly over the Amundsen–Bellingshausen Sea. The anomalous northerly wind to the east of this high pressure center over the Amundsen–Bellingshausen Sea advects warmer air into central West Antarctica, consistent with the positive isotope anomalies there. The regression map based on the Atlantic SST index also shows that SLP increases over the Amundsen–Bellingshausen Sea during the positive phase of Atlantic variability (Fig. 8, top right). Compared to the regression map based on the Pacific index, the center of high pressure anomaly is displaced southwestward and the cold advection is more pronounced in the peninsula and eastern West Antarctica, consistent with the negative isotope anomalies in these regions. This high pressure anomaly associated with Atlantic variability appears to be part of the wave train emanating from the western tropical Pacific analogous to the PSA pattern, although the island stations in the western tropical Pacific do not exhibit a very coherent pattern of precipitation anomalies.

To test the hypothesis of tropical forcing of Antarctic climate variability on decadal–interdecadal time scales, we regressed the global SLP, surface air temperature, and precipitation fields simulated in the CAM3 GOGA and TOGA runs onto the Pacific and Atlantic SST indices for the same period after 1957 (Fig. 8, top and bottom middle). The CAM3 successfully simulates the positive SLP anomalies over the Amundsen–Bellingshausen Sea during the positive phase of Pacific and Atlantic interdecadal variability when forced with the observed monthly SSTs over the global domain (GOGA run; Fig. 8, top middle). As in the observations, the center of high pressure anomaly is displaced southwestward in the regression map based on the Atlantic SST index compared to that based on the Pacific index. The simulated high pressure anomalies are too zonally elongated compared to observations, but the large-scale pattern of SLP anomalies is well reproduced in the Southern Hemisphere. Similar to the observations, negative SLP anomalies are found to the west and northwest of these high pressure anomalies in the regression maps based on the Pacific and Atlantic indices, respectively. The surface air temperature anomalies are consistent with the isotope anomalies over Antarctica. Note that the large surface air temperature anomalies off the Antarctic coast is due to the fact that sea ice anomalies are prescribed in the GOGA run.

The extratropical atmospheric anomalies in the GOGA run are linked to large-scale patterns of precipitation anomalies in the tropics (Fig. 8, top middle). During the positive phase of Pacific interdecadal variability, precipitation increases in the equatorial Pacific and decreases in the northwest and southwest tropical Pacific, consistent with observational results based on limited island station data. During the positive phase of Atlantic interdecadal variability, precipitation increases in the northern tropical Atlantic and decreases in the southern tropical Atlantic in association with the meridional dipole pattern of SST anomalies. The positive precipitation anomaly extends westward into the northern tropical Pacific. Precipitation also increases in the western-central equatorial Pacific and decreases in the southeast tropical Pacific in response to weak SST warming and cooling in these regions. Compared to the regression map based on the Pacific SST index, positive precipitation anomalies are confined north of the equator in the Pacific. The island station precipitation data are too sparse to verify the simulated pattern of tropical Pacific precipitation anomalies associated with Atlantic variability, but cloudiness anomalies based on shipboard observations (Woodruff et al. 2011) provide some support (not shown).

When the observed SST is prescribed only in the tropics (TOGA run; Fig. 8, bottom middle), the CAM3 simulates SLP anomaly patterns similar to those in the GOGA run, suggesting that a large part of the extratropical atmospheric circulation changes in the GOGA run are forced by tropical SST anomalies. The patterns of surface air temperature anomalies are also similar over West Antarctica between the GOGA and TOGA runs. There are, however, some differences in the location and amplitude of SLP anomalies in the Southern Hemisphere between the GOGA and TOGA runs. In particular, the shift of the high pressure anomaly centers over the Amundsen–Bellingshausen Sea between the Pacific and Atlantic variability is less pronounced in the TOGA run compared to the GOGA run. These differences may arise from weaker SST anomalies in

the southwest tropical Pacific between 20° and 30°S in TOGA compared to GOGA (recall section 2d). Over the southwestern tropical Pacific, the negative precipitation anomalies associated with negative SST anomalies do not extend as far south, and the high pressure anomalies are weaker in the TOGA run than in the GOGA run. Schneider et al. (2012a) suggest that the extratropical atmospheric circulation in the Southern Hemisphere is sensitive to the precipitation anomalies in this region. This hypothesis needs to be tested by widening the tropical band in the TOGA experiment.

The regression analysis of the TOGA run is extended for the entire twentieth century to validate that the same teleconnection mechanism is at work prior to 1957 (Fig. 8, bottom row). The regression pattern based on the Pacific SST index is very similar to that for the period after 1957. However, in the regression map based on the Atlantic SST index, the precipitation anomalies in the tropical Pacific and the SLP anomalies in the Southern Hemisphere are much smaller compared to those for the recent period and the high pressure anomaly is centered east of the Antarctic Peninsula. This discrepancy may be due to smaller ocean–atmosphere anomalies in the tropical Pacific associated with Atlantic interdecadal variability before 1957 (not shown) in addition to the issue with the experimental setting of the TOGA run.

The regression analysis presented in Fig. 8 has been repeated for seasonal-mean data. In the observations, the Southern Hemispheric circulation anomalies associated with Pacific and Atlantic interdecadal variability are evident from fall through spring and similar to those based on the annual-mean data (not shown), consistent with the analysis of interannual variability (e.g., Jin and Kirtman 2009; Schneider et al. 2012b). CAM3 simulates this observed seasonality for Atlantic interdecadal variability, but the seasonal dependence is less clear for Pacific variability.

We have also analyzed the GOGA and TOGA ensemble simulations with the Geophysical Fluid Dynamics Laboratory (GFDL) atmospheric GCM (AM2), which are available for 1870–2004 and 1950–2000, respectively. The results are very similar to those of CAM3 (not shown). In the AM2 GOGA run, the atmospheric teleconnection patterns are similar between 1900–99 and 1957–99 for both Pacific and Atlantic oscillations.

5. Extending the analysis of Antarctic–tropical linkages to the nineteenth century

The analysis of ice core and various instrumental data reveals strong linkages between Antarctic and tropical climate variability on decadal–interdecadal time scales during the twentieth century. In this final results section,

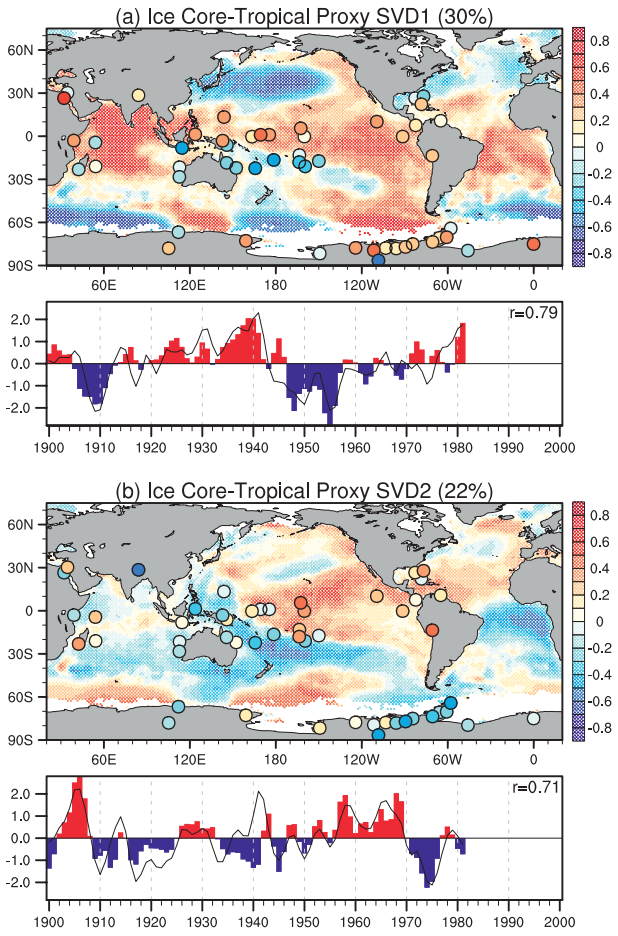

FIG. 9. (a) Pattern and time series associated with the first SVD mode of ice core and tropical proxy records for 1900–81. This mode explains 30% of the total squared covariance. Map shows correlations of tropical proxy records (circles in the tropics) and SSTs (shading) upon the ice core expansion coefficient and correlations of ice core records (circles in Antarctica) upon the tropical proxy expansion coefficient. Standardized time series of the ice core and tropical proxy expansion coefficients are shown by the color bars and black curve, respectively. These time series are correlated at a coefficient of 0.79. (b) As in (a) but for the second SVD mode, which explains 22% of the total squared covariance. Time series of the expansion coefficients are correlated at a coefficient of 0.71.

we extend the analysis further back in time using a set of ice core and various tropical proxy records available from 1799 to examine if the same Antarctic–tropical linkages exist during the nineteenth century.

Before extending the analysis to the nineteenth century, we first verify that a set of tropical proxy records can capture Pacific and Atlantic interdecadal variability and their linkages to Antarctic climate during the twentieth century. As in section 3b, the SVD analysis is conducted for 1900–81 using 17 ice core records but replacing tropical SSTs with 35 tropical proxy records. Figure 9 shows the time series of expansion coefficients

and the heterogeneous correlation maps based on these expansion coefficients for the first and second SVD modes. In the correlation maps, the ice core expansion coefficients are also correlated with global SSTs. These two leading modes explain 30% and 22% of the total squared covariance and the expansion coefficients of ice core and tropical proxy data are highly correlated (r = 0.79 for the first mode and $r = 0.71$ for the second mode). The time series of ice core coefficients and the SST correlation patterns bear a striking resemblance to those for the leading SVD modes of ice core and tropical SST (Fig. 7). The first and second SVD modes again represent Pacific and Atlantic interdecadal variability, respectively. Compared to the SVD analysis of ice core and tropical SST, the first SVD mode shows weaker positive SST correlation in the northern tropical Pacific and the phase shift in the late 1970s is less clear in the ice core coefficient. For the second SVD mode, the expansion coefficient of tropical proxy data has a strong positive peak around 1941–42, out of phase with that of the ice core data.

The correlation patterns of tropical proxy data are consistent with the correlation patterns of SST over the ocean except in the western Indian Ocean for both first and second SVD modes (Fig. 9). For the first SVD mode the coral records in the western tropical Pacific exhibit a distinct meridional dipole pattern of correlations in association with the anomalous meridional SST gradient and resultant shift of the SPCZ. The coral records from the northern Red Sea (Ras Umm Sidd) and the western equatorial Indian Ocean (Malindi), which are known to show strong signals of Pacific interdecadal variability (Felis et al. 2000; Cole et al. 2000), are also significantly correlated with the ice core coefficient of the first SVD mode. For the second SVD mode coral records show a coherent pattern of positive correlation in the central tropical Pacific. Most coral records in the southwest tropical Pacific exhibit negative correlations similar to but weaker than in the correlation map for Pacific variability. The tropical ice core record from the Andes (Quelccaya) and tree ring record from Nepal also have significant correlations with the ice core coefficient of the second SVD mode. Among the four proxy records from the tropical Atlantic, only the coral record from Bahamas exhibits significant correlation with the ice core coefficient of the second SVD mode.

We now extend the SVD analysis of ice core and tropical proxy for 1799–1981 using 6 ice core and 18 tropical proxy records. The first and second modes are presented in Fig. 10. In the heterogeneous correlation maps, the ice core expansion coefficients are correlated with global SSTs only during the overlapping period of 1870–1981. The first SVD mode explains 52% of the total squared covariance and again represents Pacific interdecadal variability. The correlation map is very similar to that of the first SVD mode for 1900–81 (Fig. 9), although the correlations are generally weaker. As in Fig. 9, positive isotope anomalies in the central West Antarctic ice cores are associated with negative anomalies in the southwest tropical Pacific coral records. There are no coral records available for the entire nineteenth century over the western equatorial Pacific where a coherent pattern of positive correlations is found in the SVD analysis for 1900–81. The expansion coefficients of ice core and tropical proxy data are correlated at a coefficient of 0.5, significant but much weaker than in the SVD analysis for 1900–81 ($r = 0.79$). Potential dating errors that increase in the coral records going back in time (Wilson et al. 2010) may partly contribute to the weaker correlations. The time series of expansion coefficients suggest that the Pacific interdecadal variability was weaker and more variable during the first half of the nineteenth century, consistent with previous studies of Pacific climate reconstruction (e.g., Biondi et al. 2001; D'Arrigo et al. 2005; D'Arrigo and Wilson 2006).

The second SVD mode explains 21% of the total squared covariance, and the expansion coefficients of ice core and tropical proxy data are correlated at a coefficient of 0.47 (Fig. 10). The correlation map bears some resemblance to that of the second SVD mode for 1900–81 (e.g., Atlantic interdecadal variability; Fig. 9). However, the correlations are insignificant except for a few proxy records and SSTs in very limited regions. The expansion coefficients are positively correlated with those of the second SVD mode for 1900–81 during the overlapping period, but the rapid shift from a positive to negative phase in the early 1970s is absent. As shown in the previous sections and in the SVD analysis of ice core and tropical proxy for 1900–81, the largest signals of Atlantic interdecadal variability are found in the ice cores from the Antarctic Peninsula and eastern West Antarctica and the coral records from the central tropical Pacific. Most of these ice core and coral records are unavailable for the nineteenth century, and thus Atlantic interdecadal variability is poorly represented in the SVD analysis of ice core and tropical proxy records for 1799–1981.

6. Summary and discussion

Due to the sparseness and short duration of meteorological observations, Antarctic climate variability is poorly understood beyond interannual time scales. In this study, we utilized a network of annually resolved ice core records and analyzed patterns and causes of

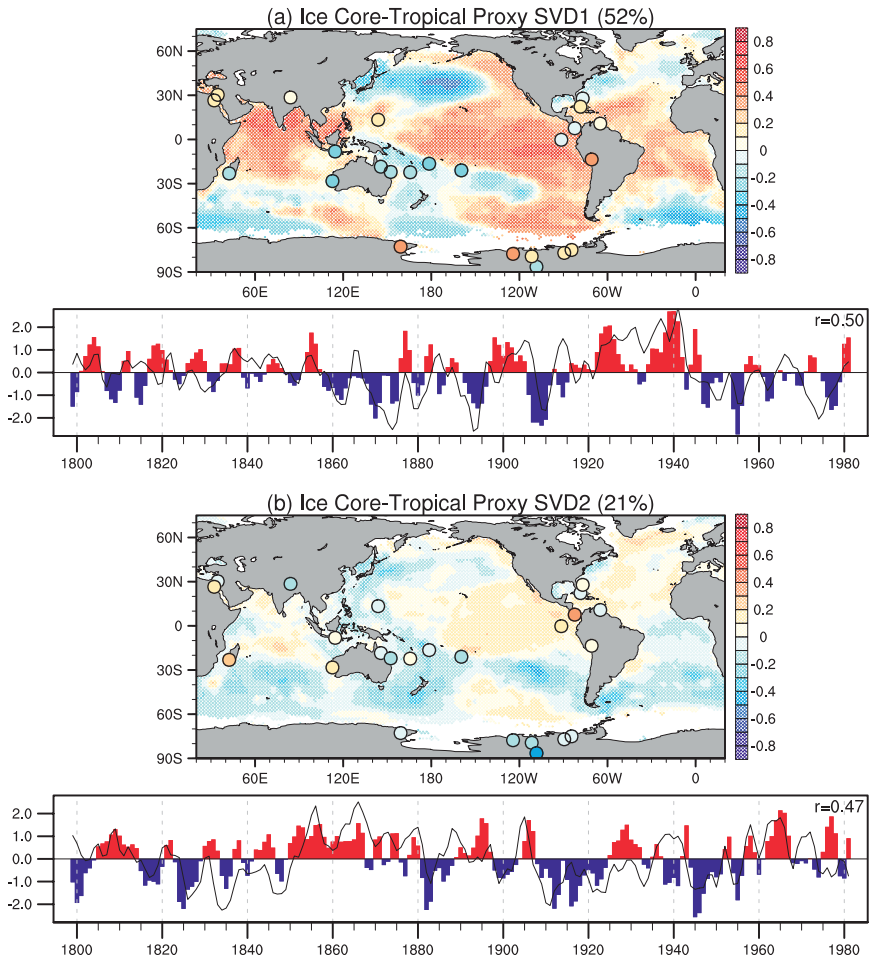

FIG. 10. As in Fig. 9 but for the first and second SVD modes of ice core and tropical proxy records for 1799–1981, which explain 52% and 21% of the total squared covariance, respectively. SSTs are correlated with the ice core expansion coefficient only for 1870–1981. Time series of the expansion coefficients are correlated at coefficients of 0.50 and 0.47 for the first and second SVD modes, respectively.

decadal–interdecadal climate variability over Antarctica for the nineteenth and twentieth centuries. The analysis of ice core and various instrumental data indicates strong linkages between Antarctic and tropical climate variability during the twentieth century. In particular, the ice core records in central West Antarctica are positively correlated with Pacific interdecadal variability, and the ice cores in the Antarctic Peninsula and eastern West Antarctica are negatively correlated with Atlantic interdecadal variability. These Antarctic–tropical linkages are robust and are recovered in various statistical methodologies such as simple correlation analysis and objective SVD analysis.

The isotope anomalies in the Antarctic Peninsula and West Antarctic ice cores are consistent with the associated changes in atmospheric circulation and implied thermal advection. The analysis of atmospheric GCM experiments suggests that tropical precipitation changes accompanying Pacific and Atlantic interdecadal variability forces atmospheric Rossby waves similar to the PSA pattern into the extratropical Southern Hemisphere, inducing surface air temperature anomalies in the peninsula and West Antarctica. A high pressure anomaly develops over the Amundsen–Bellingshausen Sea during the positive phase of both Pacific and Atlantic interdecadal variability. Because of a slight shift in the center of this high pressure anomaly, anomalous warm advection is pronounced in central West Antarctica during the positive phase of Pacific interdecadal variability while anomalous cold advection is prominent in the Antarctic Peninsula and eastern West Antarctica during the positive phase of Atlantic interdecadal variability. More diagnostic studies are needed to understand what causes the different patterns of atmospheric

teleconnections between Pacific and Atlantic interdecadal variability. Although we attempted to explain the decadal atmospheric teleconnections in terms of steady response to decadal–interdecadal tropical SST changes in this study, they may also reflect slow modulations of interannual ENSO and associated atmospheric teleconnection for Pacific variability (e.g., Bromwich et al. 2000; Turner 2004; Fogt and Bromwich 2006).

The tropical Pacific precipitation anomalies appear to be important in forcing the atmospheric circulation anomalies over the Amundsen–Bellingshausen Sea not only for Pacific variability but also for Atlantic variability. It is not clear what causes these Pacific anomalies associated with Atlantic interdecadal variability. Kushnir et al. (2010) show that a change in tropical Atlantic precipitation affects atmospheric deep convection in the tropical Pacific through adjustments of the Walker circulation. Modeling studies of paleoclimate variations during the last glacial–deglacial period also suggest that both atmospheric and oceanic teleconnections can convey the Atlantic changes to the Pacific (e.g., Dong and Sutton 2002; Vellinga and Wood 2002; Zhang and Delworth 2005; Timmermann et al. 2007; Wu et al. 2008; Xie et al. 2008; Okumura et al. 2009). Timmermann et al. (2010) show that many climate models simulate a low pressure anomaly over the Amundsen–Bellingshausen Sea in response to a slowdown of the Atlantic thermohaline circulation and associated negative dipole pattern of Atlantic SST anomalies, consistent with our analysis of interdecadal variability. This low pressure anomaly cannot be explained without small changes in tropical Pacific SSTs in their atmospheric model experiments. Thus, weak SST anomalies in the central tropical Pacific accompanying Atlantic interdecadal variability may play a crucial role in forcing an atmospheric Rossby wave to Antarctica. Recent studies suggest a strong linkage between the central tropical Pacific SST and Southern Hemispheric atmospheric circulation (Lee et al. 2010; Ding et al. 2011). The relative importance of tropical Atlantic and Pacific SSTs and the mechanism of their linkages on decadal–interdecadal time scales need to be explored further in future.

The set of ice core and tropical proxy records used in this study can capture the climate variations associated with Pacific and Atlantic decadal–interdecadal variability during the twentieth century surprisingly well. The subset of records that extend back to the nineteenth century also exists in the regions where climate signals associated with Pacific interdecadal variability are strong. These ice core and tropical proxy records can be used to reconstruct the Pacific climate variations before the instrumental period. However, the nineteenth-century subset of ice core and tropical proxy records is too sparse to fully resolve climate variations associated with Atlantic interdecadal variability. Based on the twentieth-century analysis, we suggest that more ice core records from the peninsula and eastern West Antarctica and coral and other proxy records from the central tropical Pacific as well as from the tropical Atlantic (see also similar recommendations in Wilson et al. 2010) may help to reconstruct the Southern Hemispheric climate signals associated with Atlantic interdecadal variability.

We note that the set of ice core records used in this study is primarily located over the Antarctic Peninsula and West Antarctica and thus may focus on the linkages to tropical Pacific SSTs and associated PSA teleconnection pattern, dismissing possible teleconnections between the tropics and East Antarctica. Based on a detailed analysis of Antarctic station temperature and ice core records, Schneider et al. (2012b) suggest that temperature variations over East Antarctica are largely controlled by the SAM, which is in turn significantly influenced by tropical SSTs only during summer. Due to this short seasonal window, tropical signals may not be preserved well in East Antarctic ice core records. On the other hand, the PSA teleconnections are evident from fall through spring, clearly imprinted in many ice core records from the peninsula and West Antarctica (Schneider et al. 2012b).

Both Pacific and Atlantic interdecadal variability underwent major shifts in their phases during the second half of the twentieth century (Fig. 6). The shift toward a positive phase of Pacific variability in the late 1970s is likely to have contributed to the warming of central West Antarctica and the shift toward a negative phase of Atlantic variability in the early 1970s to the warming of the Antarctic Peninsula and eastern West Antarctica via atmospheric Rossby waves and associated thermal advection as indicated by the results shown in Fig. 8. Indeed, the ice core records from these regions exhibit strong positive trends during the second half of the twentieth century (Fig. 6), whereas the trends are weaker and show less coherent pattern for the entire twentieth century (not shown). Thus, interdecadal climate variability might have contributed to the significant warming trend over the peninsula and West Antarctica suggested from the analysis of instrumental data during the past 50 years (Steig et al. 2009; Schneider et al. 2012a).

Our results point to the difficulty in separating forced climate signals from low-frequency climate variations in short Antarctic observational records. Another difficulty comes from the possibility that the tropical climate response to anthropogenic forcing may project onto the patterns of natural climate variability. For example, it is suggested that stronger anthropogenic aerosol cooling in the Northern Hemisphere than in the Southern Hemisphere resulted in asymmetric warming between the

North and South Atlantic and southward displacement of the Atlantic ITCZ during the twentieth century (e.g., Rotstayn and Lohmann 2002; Biasutti and Giannini 2006; Chang et al. 2011). In the tropical Pacific, observational and modeling studies suggest that the Walker circulation weakens in response to greenhouse gas increases, although it remains controversial whether the atmospheric circulation change is accompanied by a change in the zonal SST gradient (e.g., Vecchi et al. 2006, 2008; DiNezio et al. 2009; Deser et al. 2010b; Tokinaga et al. 2012a,b, manuscript submitted to *Nature*; Ma et al. 2012). The associated changes in the tropical precipitation pattern are, in turn, likely to force atmospheric Rossby waves into the extratropics (Deser et al. 2012), affecting the regional pattern of climate change over Antarctica. Climate proxy records can be powerful tools to analyze climate variability and change where long instrumental records are not available. The analysis of Antarctic ice core records presented in this study will serve as a basis for continued assessment of Antarctic climate change in the past and future.

Acknowledgments. We thank Alexander Tudhope for generously allowing us to use several unpublished coral records and Jian Lu for providing the GFDL AM2 simulations. We would also like to thank Mike Wallace, Qinghua Ding, Laurent Terray, Paul Kushner, and Axel Timmermann for useful discussions and Dennis Shea for technical assistance during the course of this study. Comments and suggestions by Qinghua Ding and two anonymous reviewers helped to improve the manuscript. The CAM3 simulations were conducted by Adam Phillips at NCAR and made available on the CESM Climate Variability and Change Working Group's webpage (http://www.cesm.ucar.edu/working_groups/Climate/). The following datasets were obtained online: HadISST and HadSLP2 from the Met Office Hadley Center (http://www.metoffice.gov.uk/hadobs/); land station precipitation from the Climate Research Unit of the University of East Anglia (http://www.cru.uea.ac.uk/); and Cariaco Basin G. bulloides abundance data and Bahamas coral SST reconstruction from the NOAA National Climatic Data Center Paleoclimatology Branch (http://www.ncdc.noaa.gov/paleo/paleo.html). Y. M. Okumura and D. P. Schneider were supported by a grant from the National Science Foundation Office of Polar Programs (ANT-0838871).

REFERENCES

Allan, R. J., and T. J. Ansell, 2006: A new globally complete monthly historical gridded mean sea level pressure dataset (HadSLP2): 1850–2004. *J. Climate,* **19,** 5816–5842.

Arblaster, J. M., and G. A. Meehl, 2006: Contributions of external forcings to southern annular mode trends. *J. Climate,* **19,** 2896–2905.

Biasutti, M., and A. Giannini, 2006: Robust Sahel drying in response to late 20th century forcings. *Geophys. Res. Lett.,* **33,** L11706, doi:10.1029/2006GL026067.

Biondi, F., A. Gershunov, and D. R. Cayan, 2001: North Pacific decadal climate variability since 1661. *J. Climate,* **14,** 5–10.

Black, D. E., L. C. Peterson, J. T. Overpeck, A. Kaplan, M. N. Evans, and M. Kashgarian, 1999: Eight centuries of North Atlantic Ocean atmosphere variability. *Science,* **286,** 1709–1713.

Bretherton, C. S., C. Smith, and J. M. Wallace, 1992: An intercomparison of methods for finding coupled patterns in climate data. *J. Climate,* **5,** 541–560.

Bromwich, D. H., A. N. Rogers, P. Kållberg, R. I. Cullather, J. W. C. White, and K. J. Kreutz, 2000: ECMWF analyses and reanalyses depiction of ENSO signal in Antarctic precipitation. *J. Climate,* **13,** 1406–1420.

——, A. J. Monaghan, and Z. Guo, 2004: Modeling the ENSO modulation of Antarctic climate in the late 1990s with the Polar MM5. *J. Climate,* **17,** 109–132.

Cai, W., and T. Cowan, 2007: Trends in Southern Hemisphere circulation in IPCC AR4 models over 1950–99: Ozone depletion versus greenhouse forcing. *J. Climate,* **20,** 681–693.

Chang, C.-Y., J. C. H. Chiang, M. F. Wehner, A. Friedman, and R. Ruedy, 2011: Sulfate aerosol control of tropical Atlantic climate over the twentieth century. *J. Climate,* **24,** 2540–2555.

Chang, P., L. Ji, and H. Li, 1997: A decadal climate variation in the tropical Atlantic Ocean from thermodynamic air-sea interactions. *Nature,* **385,** 516–518.

Chapman, W. L., and J. E. Walsh, 2007: A synthesis of Antarctic temperatures. *J. Climate,* **20,** 4096–4117.

Chen, J. L., C. R. Wilson, D. D. Blankenship, and B. D. Tapley, 2009: Accelerated Antarctic ice loss from satellite gravity measurements. *Nat. Geosci.,* **2,** 859–862.

Chylek, P., C. K. Folland, G. Lesins, and M. K. Dubey, 2010: Twentieth century bipolar seesaw of the Arctic and Antarctic surface air temperatures. *Geophys. Res. Lett.,* **37,** L08703, doi:10.1029/2010GL042793.

Cole, J. E., R. B. Dunbar, T. R. McClanahan, and N. A. Muthiga, 2000: Tropical Pacific forcing of decadal SST variability in the western Indian Ocean over the past two centuries. *Science,* **287,** 617–619.

Collins, W. D., and Coauthors, 2006: The formulation and atmospheric simulation of the Community Atmosphere Model Version 3 (CAM3). *J. Climate,* **19,** 2144–2161.

Comiso, J. C., 2000: Variability and trends in Antarctic surface temperatures from in situ and satellite infrared measurements. *J. Climate,* **13,** 1674–1696.

D'Arrigo, R., and R. Wilson, 2006: On the Asian expression of the PDO. *Int. J. Climatol.,* **26,** 1607–1617.

——, and Coauthors, 2005: Tropical-North Pacific climate linkages over the past four centuries. *J. Climate,* **18,** 5253–5265.

Delworth, T. L., and M. E. Mann, 2000: Observed and simulated multidecadal variability in the Northern Hemisphere. *Climate Dyn.,* **16,** 661–676.

Deser, C., and A. S. Phillips, 2009: Atmospheric circulation trends, 1950–2000: The relative roles of sea surface temperature forcing and direct atmospheric radiative forcing. *J. Climate,* **22,** 396–413.

——, ——, and J. W. Hurrell, 2004: Pacific interdecadal climate variability: Linkages between the tropics and North Pacific during boreal winter since 1900. *J. Climate,* **17,** 3109–3124.

——, M. A. Alexander, S.-P. Xie, and A. S. Phillips, 2010a: Sea surface temperature variability: Patterns and mechanisms. *Annu. Rev. Mar. Sci.,* **2,** 115–143.

——, A. S. Phillips, and M. A. Alexander, 2010b: Twentieth century tropical sea surface temperature trends revisited. *Geophys. Res. Lett.,* **37,** L10701, doi:10.1029/2010GL043321.

——, ——, V. Bourdette, and H. Teng, 2012: Uncertainty in climate change projections: The role of internal variability. *Climate Dyn.,* **38,** 527–546, doi:10.1007/s00382-010-0977-x.

DiNezio, P. N., A. C. Clement, G. A. Vecchi, B. J. Soden, B. P. Kirtman, and S.-K. Lee, 2009: Climate response of the equatorial Pacific to global warming. *J. Climate,* **22,** 4873–4892.

Ding, Q., E. J. Steig, D. S. Battisti, and M. Küttel, 2011: Winter warming in West Antarctica caused by central tropical Pacific warming. *Nat. Geosci.,* **4,** 398–403, doi:10.1038/NGEO1129.

Dong, B.-W., and R. T. Sutton, 2002: Adjustment of the coupled ocean–atmosphere system to a sudden change in the thermohaline circulation. *Geophys. Res. Lett.,* **29,** 1728, doi:10.1029/2002GL015229.

Enfield, D. B., A. M. Mestas-Nuñez, and P. J. Trimble, 2001: The Atlantic multidecadal oscillation and its relation to rainfall and river flow in the continental U. S. *Geophys. Res. Lett.,* **28,** 2077–2080.

Felis, T., J. Pätzold, Y. Loya, M. Fine, A. H. Nawar, and G. Wefer, 2000: A coral oxygen isotope record from the northern Red Sea documenting NAO, ENSO, and North Pacific teleconnections on Middle East climate variability since the year 1750. *Paleoceanography,* **15,** 679–694.

Fisher, D. A., 2002: High-resolution multiproxy climatic records from ice cores, tree-rings, corals and documentary sources using eigenvector techniques and maps: Assessment of recovered signal and errors. *Holocene,* **12,** 401–419.

Fogt, R. L., and D. H. Bromwich, 2006: Decadal variability of the ENSO teleconnection to the high-latitude South Pacific governed by coupling with the southern annular mode. *J. Climate,* **19,** 979–997.

Garreaud, R. D., and D. S. Battisti, 1999: Interannual (ENSO) and interdecadal (ENSO-like) variability in the Southern Hemisphere tropospheric circulation. *J. Climate,* **12,** 2113–2123.

Gillett, N. P., and D. W. J. Thompson, 2003: Simulation of recent Southern Hemisphere climate change. *Science,* **302,** 273–275, doi:10.1126/science.1087440.

Guan, B., and S. Nigam, 2009: Analysis of Atlantic SST variability factoring interbasin links and the secular trend: Clarified structure of the Atlantic multidecadal oscillation. *J. Climate,* **22,** 4228–4240.

Hulme, M., T. J. Osborn, and T. C. Johns, 1998: Precipitation sensitivity to global warming: Comparison of observations with HadCM2 simulations. *Geophys. Res. Lett.,* **25,** 3379–3382.

Jin, D., and B. P. Kirtman, 2009: Why the Southern Hemisphere ENSO responses lead ENSO. *J. Geophys. Res.,* **114,** D23101, doi:10.1029/2009JD012657.

Jouzel, J., and Coauthors, 1997: Validity of the temperature reconstruction from water isotopes in ice cores. *J. Geophys. Res.,* **102,** 26 471–26 487.

Karoly, D. J., 1989: Southern Hemisphere circulation features associated with El Niño–Southern Oscillation events. *J. Climate,* **2,** 1239–1252.

Kidson, J. W., 1999: Principal modes of Southern Hemisphere low-frequency variability obtained from NCEP–NCAR reanalyses. *J. Climate,* **12,** 2808–2830.

Kushnir, Y., R. Seager, M. Ting, N. Naik, and J. Nakamura, 2010: Mechanisms of tropical Atlantic SST influence on North American precipitation variability. *J. Climate,* **23,** 5610–5628.

Kwok, R., and J. C. Comiso, 2002: Spatial patterns of variability in Antarctic surface temperature: Connections to the Southern Hemisphere annular mode and the Southern Oscillation. *Geophys. Res. Lett.,* **29,** 1705, doi:10.1029/2002GL015415.

Lau, N.-C., and M. J. Nath, 1994: A modeling study of the relative roles of tropical and extratropical SST anomalies in the variability of the global atmosphere–ocean system. *J. Climate,* **7,** 1184–1207.

Lee, T., and Coauthors, 2010: Record warming in the South Pacific and western Antarctica associated with the strong central-Pacific El Niño in 2009–10. *Geophys. Res. Lett.,* **37,** L19704, doi:10.1029/2010GL044865.

Limpasuvan, V., and D. L. Hartmann, 2000: Wave-maintained annular modes of climate variability. *J. Climate,* **13,** 4414–4429.

Lythe, M. B., and Coauthors, 2001: BEDMAP: A new ice thickness and subglacial topographic model of Antarctica. *J. Geophys. Res.,* **106,** 11 335–11 351.

Ma, J., S.-P. Xie, and Y. Kosaka, 2012: Mechanisms for tropical tropospheric circulation change in response to global warming. *J. Climate,* **25,** 2979–2994.

Mantua, N. J., S. R. Hare, Y. Zhang, J. M. Wallace, and R. C. Francis, 1997: A Pacific interdecadal climate oscillation with impacts on salmon production. *Bull. Amer. Meteor. Soc.,* **78,** 1069–1079.

Marshall, G. J., 2007: Half-century seasonal relationships between the southern annular mode and Antarctic temperatures. *Int. J. Climatol.,* **27,** 373–383, doi:10.1002/joc.1407.

Miller, R. L., G. A. Schmidt, and D. T. Shindell, 2006: Forced annular variations in the 20th century intergovernmental panel on climate change fourth assessment report models. *J. Geophys. Res.,* **111,** D18101, doi:10.1029/2005JD006323.

Mo, K. C., 2000: Relationships between low-frequency variability in the Southern Hemisphere and sea surface temperature anomalies. *J. Climate,* **13,** 3599–3610.

——, and M. Ghil, 1987: Statistics and dynamics of persistent anomalies. *J. Atmos. Sci.,* **44,** 877–902.

Nobre, P., and J. Shukla, 1996: Variations of sea surface temperature, wind stress, and rainfall over the tropical Atlantic and South America. *J. Climate,* **9,** 2464–2479.

Noone, D., 2008: The influence of midlatitude and tropical overturning circulation on the isotopic composition of atmospheric water vapor and Antarctic precipitation. *J. Geophys. Res.,* **113,** D04102, doi:10.1029/2007JD008892.

Okumura, Y., S.-P. Xie, A. Numaguti, and Y. Tanimoto, 2001: Tropical Atlantic air-sea interaction and its influence on the NAO. *Geophys. Res. Lett.,* **28,** 1507–1510.

——, C. Deser, A. Hu, A. Timmermann, and S.-P. Xie, 2009: North Pacific climate response to freshwater forcing in the subarctic North Atlantic: Oceanic and atmospheric pathways. *J. Climate,* **22,** 1424–1445.

Payne, A. J., A. Vieli, A. P. Shepherd, D. J. Wingham, and E. Rignot, 2004: Recent dramatic thinning of largest West Antarctic ice stream triggered by oceans. *Geophys. Res. Lett.,* L23401, doi:10.1029/2004GL021284.

Peel, D. A., R. Mulvaney, and B. M. Davison, 1988: Stable isotope/air temperature relationships in ice cores from Dolleman

Island and the Palmer Land Plateau, Antarctic Peninsula. *Ann. Glaciol.,* **10,** 130–136.

Polvani, L. M., D. W. Waugh, G. J. P. Correa, and S.-W. Son, 2011: Stratospheric ozone depletion: The main driver of twentieth-century atmospheric circulation changes in the Southern Hemisphere. *J. Climate,* **24,** 795–812.

Power, S., T. Casey, C. Folland, A. Colman, and V. Mehta, 1999: Inter-decadal modulation of the impact of ENSO on Australia. *Climate Dyn.,* **15,** 319–324.

Pritchard, H. D., S. R. M. Ligtenberg, H. A. Fricker, D. G. Vaughan, M. R. van den Broeke, and L. Padman, 2012: Antarctic ice-sheet loss driven by basal melting of ice shelves. *Nature,* **484,** 502–505, doi:10.1038/nature10968.

Rayner, N. A., D. E. Parker, E. B. Horton, C. K. Folland, L. V. Alexander, D. P. Rowell, E. C. Kent, and A. Kaplan, 2003: Global analyses of sea surface temperature, sea ice, and night marine air temperature since the late nineteenth century. *J. Geophys. Res.,* **108,** 4407, doi:10.1029/2002JD002670.

Ribera, P., and M. E. Mann, 2003: ENSO related variability in the Southern Hemisphere, 1948–2000. *Geophys. Res. Lett.,* **30,** 1006, doi:10.1029/2002GL015818.

Rignot, E., G. Casassa, P. Gogineni, W. Krabill, A. Rivera, and R. Thomas, 2004: Accelerated ice discharge from the Antarctic Peninsula following the collapse of Larsen B ice shelf. *Geophys. Res. Lett.,* **31,** L18401, doi:10.1029/2004GL020697.

——, J. L. Bamber, M. R. van den Broeke, C. Davis, Y. Li, W. J. van de Berg, and E. van Meijgaard, 2008: Recent Antarctic ice mass loss from radar interferometry and regional climate modeling. *Nat. Geosci.,* **1,** 106–110, doi:10.1038/ngeo102.

Rintoul, S. R., 2007: Rapid freshening of Antarctic Bottom Water formed in the Indian and Pacific oceans. *Geophys. Res. Lett.,* **34,** L06606, doi:10.1029/2006GL028550.

Rotstayn, L. D., and U. Lohmann, 2002: Tropical rainfall trends and the indirect aerosol effect. *J. Climate,* **15,** 2103–2116.

Saenger, C., A. L. Cohen, D. W. Oppo, R. B. Halley, and J. E. Carilli, 2009: Surface-temperature trends and variability in the low-latitude North Atlantic since 1552. *Nat. Geosci.,* **2,** 492–495.

Salinger, M. J., J. A. Renwick, and A. B. Mullan, 2001: Interdecadal Pacific oscillation and South Pacific climate. *Int. J. Climatol.,* **21,** 1705–1721, doi:10.1002/joc.691.

Scambos, T. A., J. A. Bohlander, C. A. Shuman, and P. Skvarca, 2004: Glacier acceleration and thinning after ice shelf collapse in the Larsen B embayment, Antarctica. *Geophys. Res. Lett.,* **31,** L18402, doi:10.1029/2004GL020670.

Schmidt, G. A., A. N. LeGrande, and G. Hoffmann, 2007: Water isotope expressions of intrinsic and forced variability in a coupled ocean-atmosphere model. *J. Geophys. Res.,* **112,** D10103, doi:10.1029/2006JD007781.

Schneider, D. P., and E. J. Steig, 2002: Spatial and temporal variability of Antarctic ice sheet microwave brightness temperatures. *Geophys. Res. Lett.,* **29,** 1964, doi:10.1029/2002GL015490.

——, and D. C. Noone, 2007: Spatial covariance of water isotope records in a global network of ice cores spanning twentieth-century climate change. *J. Geophys. Res.,* **112,** D18105, doi:10.1029/2007JD008652.

——, C. Deser, and Y. Okumura, 2012a: An assessment and interpretation of the observed warming of West Antarctica in the austral spring. *Climate Dyn.,* **38,** 323–347, doi:10.1007/s00382-010-0985-x.

——, Y. Okumura, and C. Deser, 2012b: Observed Antarctic interannual climate variability and tropical linkages. *J. Climate,* **25,** 4048–4066.

Sen Gupta, A., A. Santoso, A. S. Taschetto, C. C. Ummenhofer, J. Trevena, and M. H. England, 2009: Projected changes to the Southern Hemisphere ocean and sea ice in the IPCC AR4 climate models. *J. Climate,* **22,** 3047–3078.

Shindell, D. T., and G. A. Schmidt, 2004: Southern Hemisphere climate response to ozone changes and greenhouse gas increases. *Geophys. Res. Lett.,* **31,** L18209, doi:10.1029/2004GL020724.

Steig, E. J., and Coauthors, 2005: High-resolution ice cores from US ITASE (West Antarctica); Development and validation of chronologies and estimation of precision and accuracy. *Ann. Glaciol.,* **41,** 77–84.

——, D. P. Schneider, S. D. Rutherford, M. E. Mann, J. C. Comiso, and D. T. Shindell, 2009: Warming of the Antarctic ice-sheet surface since the 1957 International Geophysical Year. *Nature,* **457,** 459–462, doi:10.1038/nature07669.

——, Q. Ding, D. S. Battisti, and A. Jenkins, 2012: Tropical forcing of Circumpolar Deepwater inflow and outlet glacier thinning in the Amundsen Sea Embayment, West Antarctica. *Ann. Glaciol.,* **53,** 19–28, doi:10.3189/2012AoG60A110.

Thoma, M., A. Jenkins, D. Holland, and S. Jacobs, 2008: Modeling Circumpolar Deep Water intrusions on the Amundsen Sea continental shelf, Antarctica. *Geophys. Res. Lett.,* **35,** L18602, doi:10.1029/2008GL034939.

Thomas, E. R., P. F. Dennis, T. J. Bracegirdle, and C. Franzke, 2009: Ice core evidence for significant 100-year regional warming on the Antarctic Peninsula. *Geophys. Res. Lett.,* **36,** L20704, doi:10.1029/2009GL040104.

Thompson, D. W. J., and J. M. Wallace, 2000: Annular modes in the extratropical circulation. Part I: Month-to-month variability. *J. Climate,* **13,** 1000–1016.

——, and S. Solomon, 2002: Interpretation of recent Southern Hemisphere climate change. *Science,* **296,** 895–899.

——, ——, P. J. Kushner, M. H. England, K. M. Grise, and D. J. Karoly, 2011: Signatures of the Antarctic ozone hole in Southern Hemisphere surface climate change. *Nat. Geosci.,* **4,** 741–749, doi:10.1038/NGEO1296.

Timmermann, A., and Coauthors, 2007: The influence of a weakening of the Atlantic meridional overturning circulation on ENSO. *J. Climate,* **20,** 4899–4919.

——, and Coauthors, 2010: Towards a quantitative understanding of millennial-scale Antarctic warming events. *Quat. Sci. Rev.,* **29,** 74–85, doi:10.1016/j.quascirev.2009.06.021.

Tokinaga, H., S.-P. Xie, A. Timmermann, S. McGregor, T. Ogata, H. Kubota, and Y. M. Okumura, 2012a: Regional patterns of tropical Indo-Pacific climate change: Evidence of the Walker circulation weakening. *J. Climate,* **25,** 1689–1710.

Trenberth, K. E., G. Branstator, D. Karoly, A. Kumar, N.-C. Lau, and C. Ropelewski, 1998: Progress during TOGA in understanding and modeling global teleconnections associated with tropical sea surface temperatures. *J. Geophys. Res.,* **103,** 14 291–14 324.

Turner, J., 2004: The El Niño–Southern Oscillation and Antarctica. *Int. J. Climatol.,* **24,** 1–31.

van de Berg, W. J., M. R. van den Broeke, C. H. Reijmer, and E. van Meijgaard, 2006: Reassessment of the Antarctic surface mass balance using calibrated output of a regional atmospheric climate model. *J. Geophys. Res.,* **111,** D11104, doi:10.1029/2005JD006495.

van den Broeke, M. R., and N. P. M. van Lipzig, 2004: Changes in Antarctic temperature, wind and precipitation in response to the Antarctic Oscillation. *Ann. Glaciol.,* **39,** 199–126.

van Loon, H., and D. J. Shea, 1987: The Southern Oscillation. Part VI: Anomalies of sea level pressure on the Southern

Hemisphere and of Pacific sea surface temperature during the development of a warm event. *Mon. Wea. Rev.,* **115,** 370–379.

Vaughan, D. G., and C. S. M. Doake, 1996: Recent atmospheric warming and retreat of ice shelves on the Antarctic Peninsula. *Nature,* **379,** 328–331.

Vecchi, G. A., B. J. Soden, A. T. Wittenberg, and I. M. Held, 2006: Weakening of tropical Pacific atmospheric circulation due to anthropogenic forcing. *Nature,* **441,** 73–76.

——, A. Clement, and B. J. Soden, 2008: Examining the tropical Pacific's response to global warming. *Eos, Trans. Amer. Geophys. Union,* **89,** 81, doi:10.1029/2008EO090002.

Vellinga, M., and R. A. Wood, 2002: Global climatic impacts of a collapse of the Atlantic thermohaline circulation. *Climatic Change,* **54,** 251–267.

Villalba, R., and Coauthors, 2011: Dendroclimatology from regional to continental scales: Understanding regional processes to reconstruct large-scale climatic variations across the western Americas. *Dendroclimatology: Progress and Prospects,* M. K. Hughes, T. W. Swetman, H. F. Diaz, Eds., Developments in Paleoenvironmental Research, Vol. 11, Springer, 175–227.

Wallace, J. M., C. Smith, and C. S. Bretherton, 1992: Singular value decomposition of wintertime sea surface temperature and 500-mb height anomalies. *J. Climate,* **5,** 561–576.

Weaver, A. J., O. A. Saenko, P. U. Clark, and J. X. Mitrovica, 2003: Meltwater pulse 1A from Antarctica as a trigger of the Bølling-Allerød warm interval. *Science,* **299,** 1709–1713.

Werner, M., and M. Heimann, 2002: Modeling interannual variability of water isotopes in Greenland and Antarctica. *J. Geophys. Res.,* **107,** 4001, doi:10.1029/2001JD900253.

Wilson, R., E. Cook, R. D'Arrigo, N. Riedwyl, M. N. Evans, A. Tudhope, and R. Allan, 2010: Reconstructing ENSO: The influence of method, proxy data, climate forcing and teleconnections. *J. Quat. Sci.,* **25,** 62–78.

Woodruff, S. D., and Coauthors, 2011: ICOADS release 2.5: Extensions and enhancements to the surface marine meteorological archive. *Int. J. Climatol.,* **31,** 951–967.

Wu, L., C. Li, C. Yang, and S.-P. Xie, 2008: Global teleconnections in response to a shutdown of the Atlantic meridional overturning circulation. *J. Climate,* **21,** 3002–3019.

Xie, S.-P., and J. A. Carton, 2004: Tropical Atlantic variability: Patterns, mechanisms, and impacts. *Earth Climate: The Ocean-Atmosphere Interaction, Geophys. Monogr.,* Vol. 147, Amer. Geophys. Union, 121–142.

——, Y. Okumura, T. Miyama, and A. Timmermann, 2008: Influences of Atlantic climate change on the tropical Pacific via the Central American isthmus. *J. Climate,* **21,** 3914–3928.

Yuan, X., and D. G. Martinson, 2001: The Antarctic dipole and its predictability. *Geophys. Res. Lett.,* **28,** 3609–3612.

Zhang, R., and T. L. Delworth, 2005: Simulated tropical response to a substantial weakening of the Atlantic thermohaline circulation. *J. Climate,* **18,** 1853–1860.

Zhang, Y., J. M. Wallace, and D. S. Battisti, 1997: ENSO-like interdecadal variability: 1900–93. *J. Climate,* **10,** 1004–1020.

Zwally, H. J., M. B. Giovinetto, J. Li, H. G. Cornejo, M. A. Beckley, A. C. Brenner, J. L. Saba, and D. H. Yi, 2005: Mass changes of the Greenland and Antarctic ice sheets and shelves and contributions to sea level rise: 1992-2002. *J. Glaciol.,* **51,** 509–527.